***Bacteroides intestinalis*-Driven Arabinoxylan Fermentation Mitigates Inflammatory and Metabolic Dysfunction**

Ziyu Zhou[1,8], Ka Lam Nguyen[1,8], Sijie Chen[1,8], Yuexi Wang[1], Min Li[1], David M. Bianchi[2], Weihao Ge[2], Shanny Hsuan Kuo [3,10], Salwa Gharieb[1], Emily Tung[1], Ronak Parmar[1], Jie Ji[1], Rohit Khorana[1], Ahmed Hetta[4,5], Isaac Cann[4,5], Roderick I. Mackie[4,5], Gee W. Lau[3] , Jing Yang[1], Wenyan Mei[1,5,6,7,9]

1 Department of Comparative Biosciences, University of Illinois Urbana-Champaign, Urbana, Illinois
2 National Center for Supercomputing Applications, University of Illinois Urbana-Champaign, Urbana, Illinois
3 Department of Pathobiology, University of Illinois Urbana-Champaign, Urbana, Illinois
4 Department of Animal Sciences, University of Illinois Urbana-Champaign, Urbana, Illinois
5 Carl R. Woese Institute for Genomic Biology, University of Illinois Urbana-Champaign, Urbana, Illinois
6 Division of Nutritional Sciences, University of Illinois Urbana-Champaign, Urbana, Illinois
7 Cancer Center at Illinois, University of Illinois Urbana-Champaign, Urbana, Illinois
8 These authors contributed equally to the work.
9 Lead contact
10 Current address: Department of Comparative Medicine, University of Washington, Seattle, Washington

Figure 2

Summary

Insufficient dietary fiber intake is strongly associated with gut microbiome dysfunction and an increased risk of noncommunicable diseases. Synergistic synbiotics, which pair defined microbial strains with their preferred carbohydrate substrates, offer a promising strategy to restore these functions. However, the rational design of such interventions remains challenging because of insufficient understanding of microbial fiber-degrading capacities and the host-relevant bioactivities of fermentation-derived metabolites. Here, we identify human colonic commensal *Bacteroides intestinalis* (*B. intestinalis*) as a key microbial mediator of dietary fiber-driven metabolic, immune, and neuronal benefits. We demonstrate that the synergistic interaction between *B. intestinalis* and its substrate, insoluble wheat arabinoxylan abundant in dietary fiber (inWAX), enhances the production of anti-diabetic and anti-steatotic bile acid species, anti-inflammatory and antioxidant phenolic compounds, and a spectrum of neuroactive compounds. These metabolic effects are accompanied by coordinated transcriptional remodeling in the colon and spleen implicating pathways governing circadian rhythm regulation, lipid metabolism, and immune defense. Importantly, these beneficial effects are preserved in conventionally raised mice with established high-fat diet-induced obesity, where *B. intestinalis* and inWAX improve glucose tolerance. Our findings uncover a mechanistic framework linking *B. intestinalis*-mediated fiber fermentation to gut-metabolism-immune crosstalk and establish a rational foundation for precision synbiotic design.

Introduction

The global adoption of a low-fiber Western diet has fundamentally altered gut microbiota function, contributing to the escalating burden of noncommunicable metabolic and inflammatory diseases worldwide.[1] In contrast, higher dietary fiber intake is linked to increased gut microbiome diversity and reduced risk of metabolic and inflammatory diseases.[2] Dietary fiber has been shown to lowers cholesterol, improve glucose homeostasis and weight control, and reduce the risk of colorectal cancer.[2] Emerging evidence further implicates dietary fiber in supporting cognitive function.[3,4] These important observations underscore the therapeutic potential of dietary fiber in preventing and managing noncommunicable diseases. Yet, the fiber-deficient Western diet has limited the daily consumption of fiber and caused the loss or reduction of many fiber-fermenting microbes in gut microbiota, thereby diminishing the benefits conferred by dietary fiber. This has spurred interest in microbiome-targeted interventions using dietary fibers (prebiotics), fiber-fermenting microbes (probiotics), and their combinations. Among these, synergistic synbiotics, which are rationally designed combinations of defined microbial strains and their preferred carbohydrate substrates, represent a particularly promising supplemental strategy. By enhancing microbial engraftment, persistence, and metabolic activity, synbiotics offer a means to restore gut microbial function and improve host metabolic outcomes in a targeted and durable manner. Despite their promise, the rational design of effective synbiotic interventions remains a significant challenge. Critical gaps remain in our understanding of microbial fiber-degrading capacities, substrate specificities, and the host-relevant bioactivities of fermentation-derived metabolites that mediate metabolic benefits.

The benefits of dietary fiber stem not only from its physicochemical properties but also from bioactive metabolites produced during its fermentation by gut commensal bacteria. Short-chain fatty acids (SCFAs) represent the most well-studied class of fiber-derived metabolites and exert broad benefits on immunity, intestinal barrier integrity, and metabolic homeostasis.[5-8] Emerging findings, however, suggest that many health-promoting effects of dietary fiber may be attributed to microbial metabolites other than SCFAs.[9] For instance, dietary fiber intake has been reported to increase the production of aromatic amino acid derivatives, neurotransmitters, secondary bile acids, and B vitamins.[9] These findings highlight the critical need to identify the gut microbes that produce these metabolites, the specific dietary substrates they preferentially ferment, and the mechanisms by which these metabolites influence host physiology. Addressing this gap is essential for fully harnessing the therapeutic potential of gut microbe–mediated fiber fermentation.

Here, we identify *Bacteroides intestinalis* 17393 (hereafter BI) as a key microbial mediator of dietary fiber-driven metabolic and immune benefits. BI is a member of fiber-degrading *Bacteroides* spp. of the phylum Bacteroidota, a major group of bacteria in the human adult distal gut. It was originally isolated from a healthy Japanese individual.[10] Our prior *in vitro* work demonstrates that BI harbors esterase gene-enriched polysaccharide utilization loci (EGE-PULs) capable of sensing and degrading insoluble wheat arabinoxylan (inWAX) *in vitro* to release ferulic acid, a phenolic compound with potent anti-inflammatory and antioxidant properties.[11] InWAX is a major plant cell wall polysaccharide abundant in cereals such as wheat, barley, and oats.[12] It consists of a β1-4-linked xylose backbone decorated with arabinose side chains that are esterified to hydroxycinnamic acids, such as ferulic and p-coumaric acids.[13]

We show that BI ferments inWAX *in vivo*, eliciting systemic and intestinal effects that collectively ameliorate inflammatory and metabolic disease phenotypes. The synergistic interaction between BI and inWAX selectively enhances the biotransformation of anti-diabetic and anti-steatotic bile acid species, hyocholic acid (HCA) and hyodeoxycholic acid (HDCA), as well as anti-inflammatory and antioxidant phenolic compounds**.** Importantly, these beneficial effects are preserved in mice with established high fat diet (HFD)-induced obesity, where BI and inWAX improve glucose tolerance. Our findings highlight the therapeutic potential of BI and inWAX as a novel synbiotic that prevent and treat noncommunicable diseases.

Results

BI promoted colon mucus layer formation

To determine the physiological impact of BI, we inoculated viable BI and heat-killed BI to germ-free (GF) mice fed a standard chow diet (Figure 1A, diet info is provided in Methods). The GF control mice were inoculated with vehicle alone (culture medium). Comparison of physiological responses to viable versus heat-killed BI allowed us to distinguish effects mediated by BI-derived metabolites, as heat-killed bacteria are incapable of metabolite production. Viable BI significantly reduced the cecum size and weight when compared to the vehicle control and heat-killed BI but had no effect on body weight and intestine lengths (Figure 1B and S1). Both viable BI and heat-killed BI significantly increased the percentages of goblet cells in the colon, duodenum, and ileum but not in the jejunum when compared to the vehicle control (Figure 1C and S1). Notably, viable BI induced a greater increase in the number of goblet cells than heat-killed BI in the colon (Figure 1C). However, only mice inoculated with viable BI developed a substantially thicker mucus layer in the colon (Figure 1D). These findings suggest that both BI cell wall components and metabolites jointly promote region-specific goblet cell differentiation, whereas mucus secretion is selectively stimulated by BI-derived metabolites.

BI-mediated fermentation of inWAX increased systemic level of ferulic acid

We next examined BI's capability and capacity of fermenting inWAX and releasing ferulic acid *in vivo*. GF mice were inoculated with viable BI or vehicle and fed a custom diet containing 5%, 10%, or 15% inWAX, or a control diet containing the same ingredients except that inWAX was replaced with 15% cellulose (Figure 2A). In the diets containing 5% or 10% inWAX, cellulose was proportionally added to make the total fiber 15% (Table S1). Cellulose was used as a control for non-specific fiber effect because BI lacks the enzymatic capacity to degrade it.[11] Systemic ferulic acid levels in mouse serum were compared across groups. As shown in Figure 2B, all three concentrations of inWAX in the diet led to a significant increase in systemic levels of ferulic acid when compared to cellulose, and the level of circulating ferulic acid correlated with the amount of inWAX intake. However, when the inWAX concentration was increased from 10% to 15%, there was no further significant increase in ferulic acid levels, suggesting that 10% inWAX may represent a dose close to the saturation point of BI's fermentation capacity. These results demonstrate that BI can ferment inWAX *in vivo* to release ferulic acid and elevate its systemic level, highlighting its anti-inflammatory and antioxidant potential.

BI-mediated fermentation of inWAX generated disease-protecting blood metabolome

To unbiasedly evaluate the impact of BI-mediated fermentation of inWAX on host metabolism, we performed an untargeted metabolomics analysis using serum samples from BI-inoculated mice fed 15% inWAX or 15% cellulose. Mice receiving inWAX diet showed a very distinct circulating metabolic profile from those receiving cellulose (Figure 2C), indicating that BI-mediated fermentation of inWAX shifts host metabolism. 22 known metabolites were significantly elevated by inWAX (Figure 2D, Table S2). Among them, ferulic acid is one of the most elevated metabolites, which is consistent with the observation from the targeted ferulic acid measurement (Figure 2B). In addition to ferulic acid, two additional phenolic acids that have antioxidant and anti-inflammatory properties, m-coumaric acid and syringic acid, are also increased (Figure 2D and 2E). This is accompanied by an elevated ratio of reduced glutathione (GSH) to oxidized glutathione (GSSG) (Figure 2F), a hallmark of improved cellular health and redox balance. This finding indicates that BI-mediated fermentation of inWAX improved the antioxidant and anti-inflammatory capability of the host.

Notably, four of the six most highly elevated metabolites in inWAX-fed mice were bile acids, including cholic acid (CA), taurocholic acid (TCA), tauroursodeoxycholic acid (TUDCA), and hyocholic acid (HCA) (Figure 2D and 2E). The increases in TCA and TUDCA narrowly missed statistical significance, largely due to substantial inter-individual variability within the inWAX-treated group. Importantly, both TUDCA and HCA have well-established anti-diabetic properties.[14-16]

The metabolite that showed the highest increase in inWAX-fed mice is D,L-N,N-didesmethyl-o-desmethylvenlafaxine, a derivative of venlafaxine. Venlafaxine is a serotonin-norepinephrine reuptake inhibitor and has been clinically used for treating depression and anxiety [17]. The elevation of this compound suggests the presence of an as-yet-uncharacterized venlafaxine-like metabolite induced by BI-mediated inWAX fermentation.

23 known metabolites are decreased in inWAX-treated mice (Table S2). Intriguingly, more than 56% of them are involved in lipid metabolism, including 7 derivatives of carnitine and 6 members of lysophosphatidylcholines (LPCs) (Figure 2G). Derivatives of carnitine act as a transport system to move activated fatty acids into mitochondria for β-oxidation, which is a primary energy-generating process. LPCs are bioactive signaling molecules derived from the partial hydrolysis of phosphatidylcholines and are involved in lipid signaling and cell membrane remodeling. The decrease in the circulating levels of these metabolites is presumably an indicative of improved lipid metabolism and energy homeostasis through a gut-liver-metabolism axis.

Together, these findings demonstrate that supplementation with BI and inWAX elevates systemic levels of phenolic compounds and bile acids with anti-inflammatory, antioxidant, and anti-diabetic activities, improves cellular redox balance, and reshapes lipid metabolism.

BI-mediated inWAX fermentation shifted the colonic transcriptome

Given that the colon is directly exposed to microbial metabolites, we next assessed the effect of BI-mediated inWAX fermentation on the colon transcriptome. 15% inWAX-treated mice exhibited 17 upregulated genes in the colon when compared to 15% cellulose-fed mice (Figure 3A, Table S2). Strikingly, the gene that is mostly upregulated is *cyclic AMP responsive element–binding protein 3–like 3*(*Creb3l3*), a transcriptional factor that promotes triglyceride metabolism.

Figure 2

Loss-of-function *Creb3l3* variants in humans have been associated with hypertriglyceridemia, whereas overexpression of *Creb3l3* reduces arteriosclerotic lesions in mouse models of arteriosclerosis.[18-21] Thus, an elevation of *Creb3l3* underscores the potential of BI and inWAX in protecting against hypertriglyceridemia and arteriosclerosis.

Surprisingly, 5 increased genes are core regulators of circadian rhythms (Figure 3A). *Per1*, *Per2,* and *Ciart* (also called *Chrono*) are key components of a negative feedback loop in the circadian control by inhibiting the activity of the CLOCK–BMAL1 complex, the master transcriptional activator of clock genes, whereas *Dbp and Tef* are circadian clock-controlled transcription factors in the PAR bZip family that mediate circadian clock output pathways via D-box elements (Figure 3B).[22-24] Using quantitative real-time PCR, we validated the increased expression of these genes in the colons of inWAX-treated mice (Figure 3C).

Other upregulated genes include *Hmox1*, *Fkbp5,* and *Hif3a* that respond to stress and hypoxia,[25-27] *Slc2a5* and *Abcc2* for membrane transport,[28,29] *Kyat1* for the tryptophan Kynurenine Pathway, and *Tsku* and *Lefty1* for tissue development and homeostasis.[30,31]

Only two genes were downregulated in inWAX-treated mice, including *Pou1f1*, a transcriptional factor with unknown intestinal function, and *Tac1* (Figure 3A), which encodes the precursor for neuropeptides tachykinins that regulate intestinal motility, secretion, and vascular functions.[32]

Together, these findings indicate that BI-mediated fermentation of inWAX influences intestinal function at least in part by activating genes essential for triglyceride metabolism and intestinal circadian clock.

BI-mediated inWAX fermentation protects against colitis

Given that BI-mediated fermentation of inWAX increased systemic levels of anti-inflammatory and antioxidant metabolites, we investigated its protective effect against dextran sulfate sodium (DSS)-induced colitis. BI mono-associated male mice receiving 15% inWAX or 15% cellulose were challenged with 2% DSS to induce colitis (Figure 4A, thereafter inWAX:DSS+ and Cellu;DSS+, respectively). Mice treated with 15% inWAX without DSS served as controls (inWAX;DSS-). InWAX:DSS+ mice exhibited significantly less body weight loss in response to DSS treatment when compared to Cellu;DSS+ mice (Figure 4B). At the end of the treatment, Cellu:DSS+ mice showed splenomegaly because of inflammation. This splenomegaly was substantially attenuated in inWAX;DSS+ mice (Figure 4C), suggesting reduced systemic inflammation. Consistently, inWAX:DSS+ mice displayed significantly lower colonic histopathological scores, characterized by reduced crypt dilation, fibrosis, and inflammatory infiltrates (Figure 4D).

Collectively, these results strongly indicate that BI-mediated fermentation of inWAX confers protection against DSS-induced colitis.

inWAX fermentation induced protective colon transcriptome against DSS

To elucidate the molecular basis of colitis resistance conferred by BI and inWAX, we analyzed DSS-induced transcriptional changes in the colon. Relative to Cellu;DSS+ mice, inWAX;DSS+ mice exhibited upregulation of 52 genes (Figure 5A, Table S3). This includes 7 genes involved in

innate immune defense (*Reg3b*, *Retn*, *Apol7c*, *Cd177*, *Clec14a*, *Clec2e*, *Mafb*). *Reg3b* was among the most strongly induced genes, and it encodes an antimicrobial lectin that limits bacterial translocation and protects against DSS-induced colitis,[33-35] suggesting enhanced host defense to DSS-induced colitis.

InWAX treatment induced a set of genes classically associated with male fertility, including *Svs2*, *Ddx3y*, *Uty* (*Kdm6c*), *Kdm5d*, *Eif2s3y*, and *Uba1y*. Five of these genes are Y chromosome-linked and function in RNA translation (*Eif2s3y*, *Ddx3y*), epigenetic regulation (*Uty*, *Kdm5d*), and protein ubiquitination (*Uba1y*).[36-40] *Svs2* is a non–Y-linked gene encoding a secreted seminal vesicle protein that protects sperm from immune attack,[41] with an unknown role in the intestine. This interesting finding suggests that BI-mediated inWAX fermentation induces sex-based immune modulation in the colon in response to DSS insult.

Notably, nearly half of the upregulated genes encoded metabolic regulators involved in lipid, protein, carbohydrate, and xenobiotic metabolism (Figure 5B and 5C). Most of them encode enzymes or regulators of enzymes, underscoring a broad metabolic reprogramming of the colon. Among them, lipid metabolic pathways show the strongest enrichment (Table S4), spanning multiple layers of lipid metabolism regulation, including lipid synthesis and desaturation (*Thrsp*, *Scd1*),[42,43] storage (*Plin1*),[44] hydrolysis and mobilization (*Apoc2*, *Angptl4*, *Ces1f*, *Ces1g*),[45-47] as well as extracellular regulation of lipid metabolic signaling (*Tsku*).[48] This finding highlighted a coordinated lipid metabolic reprogramming in the colon.

Importantly, many of these metabolism regulatory genes possess immune-regulatory functions. For instance, *Scd1* encodes Stearoyl-CoA desaturase-1 that converts saturated fatty acids into monounsaturated fatty acids,[43], and can attenuate DSS-induced colitis.[49] *Ido1* modulates immune responses by catabolizing tryptophan.[50-52] *Mcpt1* encodes a Mast cell protease that is predominantly expressed in intestinal mucosal mast cells and has multifaced roles in inflammation.[53] *Arg2* encodes a mitochondrial enzyme involved in arginine metabolism and nitric oxide synthesis, and can influence immune cell function and suppress inflammation.[54-57] *Vnn1* encodes a pantetheinase that converts pantetheine to pantothenate and cysteamine to enhance SCFA production and protect against DSS-induced colitis.[58] *Angptl4* represses lipoprotein lipase and is also immune regulatory.[46]

Collectively, these data indicate that BI-mediated fermentation of inWAX induces a coordinated transcriptional program that couples metabolic reprogramming with enhanced mucosal immune protection. This finding reveals a central role for gut microbiota-driven metabolic remodeling in promoting intestinal resiliency to inflammatory injury.

Consistent with attenuated inflammatory stress in inWAX-treated mice, we observed significant downregulation of genes associated with wound healing, stress responses, and cell junction assembly, along with reduced activities in MAPK signaling and PI3K-AKT signaling (Figure 5D, Table S4).

inWAX fermentation induced protective spleen architecture and transcriptome against DSS

The spleen is a major secondary lymphoid organ that integrates hematopoietic and immunological functions. Given our observation that BI-mediated fermentation of inWAX markedly attenuated

DSS-induced splenomegaly, we next examined the impact of BI-mediated inWAX fermentation on splenic architecture and transcriptional programs. Compared with cellulose-treated controls, inWAX-treated mice exhibited a pronounced expansion of the white pulp (Figure 6A), the lymphocyte-enriched compartment of the spleen, indicative of enhanced adaptive immune cell abundance. This was confirmed by transcriptome profiling, which showed broad activation of genes essential for B and T cell proliferation and differentiation, activation, immunoglobulin production, and cytokine signaling, including those encoding components of Th1, Th2, Th17, and JAK-STAT signaling pathways (Figure 6B, Table S3 and S4). In contrast, genes suppressed by inWAX treatment were enriched for DNA replication and cell cycle pathways (Figure 6C, Table S3 and S4), which presumably attenuated splenomegaly.

To define how these transcriptional changes translate into immune cell composition, we performed immune cell fraction analysis. InWAX-treated mice showed a robust expansion of adaptive immune populations, including B cells and T cells (Figure 6D and 6E, Table S5). Macrophages also had considerable expansion, although to a lesser extent compared to lymphocytes. Only a slight increase in natural killer cells was observed. In contrast, dendritic cells were reduced in inWAX-treated mouse spleen, suggesting dampened activation of pro-inflammatory innate immune circuits.

Notably, 16 genes induced in the spleen were also upregulated in the colon of inWAX-treated mice (Figure 6F). These shared genes included four Y-linked genes (*Ddx3y, Eif2s3y, Kdm5d,* and *Uty*), seven metabolic enzymes and regulators, the fructose transporter *Slc2a5*, the stem cell-associated factor *Piwil4*, and immune-related genes (*Apol7c* and *Retn*). This overlap suggests that BI-mediated inWAX fermentation activates a conserved transcriptional program in both the intestine and spleen to counteract DSS-induced inflammatory stress, revealing coordinated immune–metabolic reprogramming across local and systemic compartments. The induction of Y-linked genes in both colon and spleen further points to a potential sex-dependent component of local and systemic inflammatory stress responses.

Together, these findings indicate that BI-mediated inWAX fermentation activates adaptive immune gene programs and induces coordinated transcriptional changes across the colon and spleen in the context of DSS-induced inflammatory stress.

InWAX fermentation ameliorates HFD-induced glucose intolerance

Given that BI-mediated inWAX fermentation increased systemic levels of anti-inflammatory and antioxidant phenolic compounds and anti-diabetic bile acids, we next examined whether these beneficial effects could be preserved in the context of HFD-induced gut dysbiosis to ameliorate metabolic dysfunction in obesity. We found BI is not a native gut resident of C57BL/6J mice, and thus used this strain for the study (Figure S2A). As outlined in Figure 7A, conventionally raised male mice were first preconditioned on HFD (60 kcal% Fat) for 8-week to induce obesity and then randomly assigned to receive HFD alone (HFD), custom HFD supplemented with 10% cellulose (HFD+Cellu), or custom HFD supplemented with 10% inWAX (HFD+inWAX). Custom HFD diets were formulated by replacing ~6.5% cellulose in the standard HFD with 10% cellulose or 10% inWAX, while maintaining identical macronutrient caloric composition (Table S1) . Cellulose served as a non-fermentable fiber control to isolate inWAX-specific effects and to

control for the modest reduction in calorie density introduced by fiber inclusion (~4% less than standard HFD).

After a 5-day dietary acclimation period, mice in all three groups were orally inoculated with BI every other day for four weeks. BI was administered to the HFD and cellulose groups to control for BI-induced effects independent of fermenting inWAX. Body weight was monitored every other day during the first 12 days of treatment. While there is no significant difference in the weight gain between HFD+inWAX and HFD+Cellu mice, mice in these two groups consistently gained less weight than HFD-only control, likely reflecting reduced caloric intake associated with fiber supplementation (Figure S2B).

Glucose tolerance was assessed on day 29. HFD+inWAX mice displayed a consistent lower blood glucose level at 30-, 60-, and 90-minutes following glucose administration when compared with both HFD-only and HFD+Cellu groups, with the difference between HFD and HFD+inWAX groups at 60 minutes reaching statistical significance (Figure 7B). While cellulose-treated mice exhibited modest reductions in glucose levels relative to HFD controls, they are not statistically significant, suggesting a limited, nonspecific fiber effect. These results indicate an improvement in glucose tolerance delivered by the synergistic function of BI and WAX.

InWAX fermentation induced health-promoting bile acid species in obese mice

To define the metabolic basis underlying the health benefits conferred by inWAX fermentation in obese mice, we examined its effects on the bile acid pool. Total 26 bile acids were evaluated by targeted quantitative assay. InWAX-treated mice exhibited a marked increase in the concentrations of four bile acid species, HCA, hyodeoxycholic acid (HDCA), ω-muricholic acid (ωMCA), and deoxycholic acid (DCA) (Figure 7C; Table S6). At the level of total bile acids, both inWAX- and cellulose-treated mice showed modest increases that did not reach statistical significance. To determine whether the increases in HCA, HDCA, ωMCA, and DCA reflected selective enrichment rather than a general rise in total bile acids, their relative proportions within the total bile acid pool were compared across groups. Except for ωMCA, the proportions of HCA, HDCA, and DCA were substantially elevated, although the increase in HDCA narrowly missed statistical significance (Figure 7C and S3, Table S7). These results suggest BI and inWAX selectively enhances the production of HCA, HDCA, and DCA in obese mice.

In mice, the biosynthetic origin of HCA remains incompletely defined. HDCA and DCA are secondary bile acids generated through microbial biotransformation. HDCA can be produced via microbial 7-dehydroxylation and 6β-epimerization of αMCA and βMCA as well as 7-dehydroxylation of HCA.[59,60] To assess whether increased HDCA resulted from enhanced conversion of αMCA and βMCA, we compared the ratios of HDCA to these precursor bile acids. InWAX-fed mice exhibited a significant increase in the HDCA to αMCA and βMCA ratio compared with mice fed HFD alone, whereas this increase was not observed in cellulose-treated mice (Figure 7D). In contrast, the HDCA-to-HCA ratio was not increased in inWAX-treated mice, suggesting that BI-mediated inWAX fermentation did not enhance conversion from HCA. Together, these findings suggest that HDCA production is presumably increased primarily through enhanced microbial 7-dehydroxylation and 6-hydroxy epimerization of αMCA and βMCA.

Notably, HCA was also induced by inWAX but not cellulose in BI mono-associated mice (Figure 2D). These findings suggest that while HCA production can be directly enhanced by metabolites from BI-mediated inWAX fermentation, HDCA production requires the cooperative activity of additional gut microbial species. Importantly, both HCA and HDCA are reduced in patients with obesity, diabetes, and non-alcoholic fatty liver disease (NAFLD), and have been reported to improve glucose and lipid homeostasis and to protect against atherosclerosis.[16,61-66] The selective expansion of these bile acid species highlights the therapeutic potential of the BI-inWAX synbiotic in ameliorating HFD-induced metabolic dysfunction by restoring health-promoting bile acid signaling.

In addition, both inWAX and cellulose treatments promote an increase in bile acid deconjugation activity, as reflected by higher ratios of unconjugated to total bile acids, although the increase in cellulose-treated mice narrowly missed statistical significance (Figure 7E).

InWAX fermentation induced the fecal metabolome shift

We next used untargeted fecal metabolomics analysis to unbiasedly examine the impact of inWAX and BI on the fecal metabolome, a functional readout of microbial metabolic activity. We observed a marked remodeling of the fecal metabolic landscape in inWAX-treated mice compared with both HFD and cellulose-treated controls (Figure 8A). In total, 123 metabolites were uniquely altered by inWAX, with 85 increased and 38 decreased (Fig. 8B;Table S8), defining a distinct microbial metabolic signature induced by BI and inWAX under HFD conditions. Structurally, the metabolites exclusively upregulated by inWAX were highly enriched for amino acids and peptides (47%) (Figure 8C, Table S9). Strikingly, ~33% of them belonged to neurotransmitters and their precursors (Figure 8D), suggesting that the synbiotic effect of BI and inWAX may shift protein metabolism toward enhanced neuroactive compound production and potentially strengthen the gut-brain metabolic crosstalk. The second most enriched class comprised fatty acid derivatives, predominantly oxygenated fatty acids (oxylipins) derived from long-chain polyunsaturated fatty acids, consistent with the role of this synbiotic in rewiring lipid metabolic pathways.

In line with BI-mediated liberation of FA from inWAX, we observed a robust increase in ferulate, a salt form of FA, and its derivative dihydroisoferulic acid (Figure 8E). Notably, six other phenolic compounds with well-documented anti-inflammatory and antioxidant activities[67-69], were also significantly elevated, including simple phenolics (o-coumaric acid and 3,4-dihydroxyacetophenone), flavonoids (7-O-methyleriodictyol and jaceoside), and enterolignans (enterolactone and enterodiol). While FA and o-coumaric acid are typically ester-linked to the arabinoxylan backbone and are therefore likely direct products of inWAX fermentation, the remaining phenolic compounds represent microbial biotransformation products of dietary polyphenols. Concomitantly, multiple complex plant polyphenols were significantly reduced, among which Syringaresinol can be microbially converted to enterolactone and enterodiol.[70] These reciprocal changes indicate that the BI–inWAX synbiotic not only releases health-promoting metabolites through inWAX fermentation (e.g., FA) but also enhances microbial conversion of dietary polyphenols into bioactive metabolites. Notably, this metabolic rewiring was observed exclusively in BI-inWAX treated mice, supporting a model wherein BI-inWAX promotes cooperative, cross-feeding–dependent gut community function.

Additionally, inWAX fermentation significantly elevated nicotinic acid (vitamin B3) and pantothenate (vitamin B5) (Figure 8E), two essential cofactors for cellular energy metabolism. While nicotinic acid can be synthesized by both host and microbes, pantothenate is exclusively produced by gut microbes, further supporting a microbiota-dependent reprogramming of host metabolic capacity.

Unlike upregulated metabolites, the metabolites exclusively downregulated in InWAX-treated mice were structurally heterogeneous (Table S8). Besides the four aforementioned plant polyphenols, it includes sphingolipids and glycerophospholipids, suggesting a role of BI and inWAX in modulating lipid metabolism.

We also identified 49 metabolites altered in both inWAX- and cellulose-treated mice (35 increased, 14 decreased), likely reflecting shared fiber-dependent effects. Most of the co-upregulated metabolites are amino acids and short peptides(Table S8), indicating that both fermentable and nonfermentable dietary fiber enhanced protein metabolism. Interestingly, the co-downregulated metabolites include 6 phosphatidylcholine derivatives involved in membrane composition regulation and lipid mediator signaling pathways (Fig 8F). Notably, 3 of them, LysoPC(17:0), LPC(16:0), LysoPC (16:0), are also downregulated in the serum of inWAX-treated BI mono-associated mice, suggesting that BI-mediated inWAX fermentation has a direct role in reducing their production, and this function is preserved under the gut microbiota of HFD-induced obesity.

Additionally, 49 metabolites were uniquely altered by cellulose, with 17 increased and 32 decreased, indicating that fermentable inWAX and non-fermentable cellulose exert distinct metabolic effects under high-fat diet conditions. 8 of the 17 cellulose-upregulated metabolites were short peptides, suggesting that, despite being non-fermentable, cellulose may still influence protein metabolism, albeit through pathways distinct from those activated by fermentable inWAX. Except for a single sulfated dietary polyphenol metabolite, 3-(3-hydroxyphenyl)propionic acid sulfate, cellulose did not increase the level of beneficial phenolic compounds and bile acids as inWAX. These findings indicate that the synergistic interaction between BI and inWAX is critical for conferring the robust health-promoting effects.

Collectively, by testing the BI-inWAX effect in BI-monoassociated mice and conventionally raised mice with HFD-induced obesity, we demonstrate that the synergistic effects between BI and its preferred fiber substrate, inWAX, enhances microbial production of anti-inflammatory and antioxidant phenolic metabolites and selectively expands anti-diabetic and anti-steatotic bile acid species, HCA and HDCA. These changes are accompanied by coordinated transcriptional remodeling in both colon and spleen, implicating pathways involved in circadian regulation, lipid metabolism, and immune homeostasis. Importantly, the metabolic effects are preserved in conventionally raised mice with established HFD-induced obesity, where BI and inWAX significantly improves glucose tolerance. These findings highlight the therapeutic potential of this synbiotic to improve metabolic homeostasis in people with obesity.

Discussion

The modern low-fiber diets have driven the loss or depletion of fiber-fermenting microbes, thereby attenuating the health benefits of fiber consumption. Synergistic synbiotics, which pair defined

microbial strains with their preferred fiber substrates, offer a promising strategy to restore these functions. However, the rational design of such interventions is constrained by insufficient understanding of microbial fiber-degrading capacities and the host-relevant bioactivities of fermentation-derived metabolites.

In this study, we present compelling evidence that BI is a key microbial mediator of dietary fiber-driven metabolic, immune, and potentially neuronal benefits. We show that the synergistic interaction between BI and its dietary fiber substrate, inWAX, selectively enhances the production of anti-diabetic and anti-steatotic bile acid species, as well as anti-inflammatory and antioxidant phenolic compounds even in the context of HFD-induced gut microbiota. Further, it remodels protein metabolism toward enhanced neuroactive compound production, which potentially strengthens the gut-brain metabolic crosstalk. These microbial metabolites are accompanied by coordinated transcriptional reprogramming in the colon and spleen that improves circadian rhythm regulation, lipid metabolism, and immune defense.

A particularly notable finding is the selective expansion of health-promoting HCA, HDCA, and TUDCA. These bile acids have been shown to ameliorate metabolic disorders such as diabetes, atherosclerosis, and non-alcoholic fatty liver disease (NAFLD).[16,62-64] Reduced systemic levels of HCA and HDCA are found in individuals with obesity and diabetes, further underscoring their therapeutic relevance.[16,61] TUDCA, which is clinically approved for primary biliary cholangitis due to its cytoprotective properties, has also shown promise in obesity, IBD, and neurodegenerative diseases.[14,15,71-75] The selective expansion of these beneficial bile acids by the synergistic effects of BI and inWAX, even under HFD-induced obesity, highlights the translational potential of this synbiotic strategy for metabolic disease intervention.

Mechanistically, how BI-mediated inWAX fermentation enhances the production of these bile acid species is of great interest. In BI mono-associated mice, inWAX increased systemic TUDCA and HCA levels compared with cellulose, suggesting that BI induced TUDCA and HCA through fermenting inWAX rather than releasing extracellular enzymes. This effect likely arises from fermentation-derived metabolites that reprogram hepatic bile acid biosynthetic pathways, a mechanism that warrants further investigation

In contrast, the increase of HDCA by BI and inWAX occurs only in the presence of the complex gut microbiota, suggesting that its biotransformation needs the cooperative activity of additional gut microbial species. In mice, HDCA can be produced by microbial 7-dehydroxylation and 6-hydroxy epimerization of αMCA and βMCA.[60] The significantly increased ratio of HDCA to αMCA and βMCA in inWAX-treated mice support a model system wherein BI-inWAX provide nutrients that cross-feed gut microbes that convert αMCA and βMCA to HDCA. In line with this idea, a study in gnotobiotic rats found that a Gram-positive microbe termed HDCA-1, is capable of converting αMCA and βMCA to HDCA via 7-dehydroxylation and 6-hydroxy epimerization only in the presence of a growth factor-producing strain.[60] A more recent study in mice shows that *Bacteroides ovatus*, a member of *Bacteroides* genus, promote HDCA production by supporting the growth of 7-dehydroxylating bacterium *Clostridium scindens*.[76] Future experiments that co-culture BI and HDCA-producing microbes in the presence of inWAX could help address this model hypothesis.

In addition to selectively expanding beneficial bile acid species in HFD-induced obese mice, BI and inWAX also enhance the microbial biotransformation of dietary plant polyphenols into a spectrum of bioactive metabolites, including simple phenolics, flavonoids, and enterolignans. These compounds are well documented for their potent anti-inflammatory and antioxidant activities.[67-69] This enhanced biotransformation suggests that BI and inWAX not only generate specific metabolites such as ferulic acid with direct therapeutic potential, but also broadly augment gut microbiota-mediated metabolic processes. As a result, this synbiotic intervention substantially amplifies the host's capacity to extract and utilize the health-promoting benefits of dietary fiber.

An unexpected and conceptually important finding is the induction of core circadian clock genes in the intestine following BI-mediated inWAX fermentation. The intestinal circadian clock is critical for mucosal barrier integrity, immune responses, metabolism, and gut microbiota function. Disrupted circadian rhythm has been associated with a higher risk and more aggressive course of IBD.[77,78] Reduced colonic expression of *Per1* and *Per2* has been observed in patients with IBD,[79,80] and mice lacking these genes exhibit impaired antimicrobial secretion and heightened sensitivity to DSS-induced colitis.[81] Our findings uncover a previously unrecognized link between microbial fiber fermentation and intestinal circadian regulation, potentially connecting microbial metabolism with gut–brain–immune axis signaling.

Another interesting finding from this study is BI-mediated inWAX fermentation induces robust activation of Y-linked genes, *Ddx3y, Eif2s3y, Kdm5d,* and *Uty,* in both the colon and spleen during immune defense against DSS-induced colitis. These genes function in RNA translation and epigenetic regulation, processes essential for stress and immune responses. Their induction suggests a potential sex-biased component in the host response to fiber fermentation. Future studies examining whether BI and inWAX similarly regulate the corresponding X-linked counterparts of these genes in female mice will be essential to clarify this dimension of synbiotic responsiveness.

Together, our findings expand the prevailing paradigm of fiber-microbiota-host interactions by demonstrating that dietary fiber-driven health benefits can be mediated by microbial metabolites beyond SCFAs. Importantly, our work establishes a rational framework for the design of synergistic synbiotics, which pairs defined microbial strains with specific fiber substrates to target inflammatory and metabolic diseases. This study integrates multi-omics approaches with mono-associated gnotobiotic mouse models and conventionally raised high-fat diet-induced obese mice, which provides a comprehensive and mechanistic evaluation of host-microbe-diet interactions.

Limitation of the study

One limitation of this study is the absence of a direct assessment of inWAX fermentation independent of BI in HFD-induced obese mice. It is therefore possible that inWAX alone exerts microbiota-dependent effects that partially contribute to the effects observed in the HFD + inWAX group. However, this does not weaken our central conclusion regarding the therapeutic potential of BI and inWAX as a synergistic synbiotic. Notably, BI mono-association experiments demonstrate that BI-mediated inWAX fermentation alone is sufficient to confer multiple beneficial effects, including expansion of health-promoting bile acids, increased systemic levels of anti-inflammatory and antioxidant phenolic compounds, reprogramming of lipid metabolism, and increased local and systemic immune protection against IBD.

MATERIALS AND METHODS

Bacteria culture

Bacteroides intestinalis DSM 17393 (BI) was cultured in an anaerobic workstation (Coy Laboratory Products) as previously described.[82] Briefly, BI colonies were grown anaerobically at 37°C overnight in Brain Heart Infusion with Supplements (BHIS) medium. Bacterial growth was monitored by measuring the optical density at 600 nm (OD_{600}) using a spectrophotometer. To inoculate mice, BI was cultured anaerobically until reaching log-phase growth.

Mice

Ethics statement of animal use

All mice used in these experiments were housed at the University of Illinois Urbana Champaign (UIUC) animal care facilities and cared for according to the institutional 'Guide for the Care and Use of Laboratory Animals'. All procedures involving mouse care, euthanasia, and tissue collection were approved by the UIUC Animal Care and Use Committee (IACUC approved protocol #23096).

Diets

Custom diets were formulated by Research Diets for use in BI mono-associated and conventionally raised mice. For BI mono-associated mice, custom chow diets were formulated using an open standard diet (D11112201; Research Diets) as the base. InWAX or cellulose was added to replace the standard cellulose component, yielding diets containing 5%, 10%, or 15% inWAX (w/w). In diets containing 5% or 10% inWAX, cellulose was added proportionally to achieve a total dietary fiber content of 15% (w/w). In the diet containing 15% inWAX, cellulose was fully replaced by inWAX. For conventionally raised mice, custom HFDs were prepared using a 60% kcal fat rodent diet (D12492; Research Diets) as the base. InWAX or cellulose was added to replace the standard cellulose component, yielding diets containing 10% dietary fiber (w/w). Detailed diet compositions are provided in Table S1.

InWAX was purchased from Neogen Corporation (MI, USA; P-WAXYI; >90% purity), and cellulose was supplied by Research Diets, Inc.

BI mono-association in mice fed standard chow diet

GF mice were fed a standard chow diet (Envigo Teklad, 2019S) and orally gavaged every other day with 200 µL of BHIS medium containing live BI (2.24×10^8 CFU/mL), heat-killed BI, or BHIS medium alone (vehicle control). The absence of viable bacteria in heat-killed BI preparations was confirmed by anaerobic incubation in BHIS broth at 37°C, with growth monitored for up to 3 days. Viability of BI in mice inoculated with live BI was confirmed midway through the treatment period by quantifying colony-forming units (CFUs) from fecal samples using conventional plating on BHIS agar.

The identity and specificity of BI in colonized mice were validated by sequencing PCR amplicons generated from fecal microbial DNA using both universal 16S rRNA primers and BI strain–specific primers (sequences are provided in Table S10). Following euthanasia, intestinal length and cecum weight and length were measured. Intestinal tissues were either flash-frozen, fixed in

4% paraformaldehyde for histological analyses, or fixed in Methacarn solution (60% methanol, 30% chloroform, 10% glacial acetic acid) for mucus architecture assessment. Goblet cells and mucus were visualized in Methacarn-fixed, paraffin-embedded colon sections using Alcian Blue staining (pH 2.5).[83] Alcian Blue pH 2.5 - Brown Hopps Gram was performed by staining slides with Alcian Blue (pH 2.5) first, followed by the Brown Hopps Gram Stain procedure as described previously with slight modifications.[84] Specifically, 95% ethanol was used in place of Cellosolve as the differentiating solution.

Goblet cell quantification

A defined region of the middle colon was selected for analysis, and the same region was examined for each mouse. The relative number of goblet cells per crypt was determined by calculating the ratio of goblet cells to the total number of colonic epithelial cells within each crypt. At least 30 measurements per mouse were collected.

Colon mucus layer quantification

Measurements were performed using imageJ in distal colon regions exhibiting a continuous mucus layer ≥100 µm in length, with an intact epithelial lining and clearly defined luminal content stratification. Mucus thickness was quantified as the perpendicular distance spanning the visibly firm, dense mucus layer. For each qualifying region, a minimum of three perpendicular measurements were obtained at positions spaced 50 µm apart along the length of the mucus layer. Serial sections were collected at 50 µm intervals from each mouse to ensure that at least 30 measurements were obtained from comparable anatomical regions at different depths within the same animal. Measurements were averaged in sets of six, and these means were pooled for statistical comparisons between experimental groups.

BI mono-association in mice fed chow diet containing inWAX or cellulose

GF mice were acclimated to diets containing inWAX or cellulose for 5 days prior to BI inoculation. Mice were then orally gavaged with BI (200 µl at the concentration of 2.24×10^8 CFU/mL) every day. Body weight was monitored daily throughout the experiment. The viability and specificity of BI in colonized mice were validated by conventional plating and PCR-based sequencing as described above. Following euthanasia, tissues and serum were collected. Serum samples were processed for ferulic acid measurement or untargeted metabolomic profiling. Intestines were either flash-frozen or fixed in 4% paraformaldehyde for histological evaluation.

BI inoculation in mice fed HFD diet with or without inWAX or cellulose

14-week-old conventionally raised C57BL/6J mice preconditioned with an HFD for 8 weeks were purchased from The Jackson Laboratory (strain no. 380050). Mice were acclimated to HFDs with or without inWAX or cellulose for 5 days prior to BI inoculation. Mice were then orally gavaged with BI every other day for 28 days, followed by a glucose tolerance test as described below. Body weight was monitored every other day. BI abundance and specificity in colonized mice were confirmed by PCR and PCR-based sequencing. At the experimental endpoint, mice were fasted overnight and subsequently refed with their respective diets. Fresh fecal samples were collected 2 hours after refeeding for targeted bile acid quantification and metabolomic analyses. Following euthanasia, tissues were collected for downstream analyses.

Glucose tolerance test

Mice treated with BI and fed HFDs, with or without cellulose and inWAX, were fasted overnight and administered glucose (1 g/kg body weight) via intraperitoneal injection. Blood glucose levels were measured from tail vein blood at baseline (0 minute) and at 15-, 30-, 60-, 90-, and 120-miniutes post-injection.

DSS-induced colitis

BI mono-associated mice received either 15% inWAX or 15% cellulose were treated with 2% (w/v) dextran sulfate sodium (DSS) in drinking water for 5 days (referred to as inWAX;DSS+ and cellu;DSS+, respectively). The control mice received 15% inWAX without DSS treatment (inWAX;DSS-). All mice were maintained on their respective diets throughout the DSS or water treatment period. Body weight was monitored daily as clinical readouts of colitis. On day 5 of DSS treatment, mice were euthanized for tissue collection. A range of physical parameters were evaluated, including colon length, spleen weight, and spleen length.

For histological analyses, tissues were fixed in 4% paraformaldehyde and paraffin processed for histomorphology. Unless otherwise specified, tissue sections were cut at 5 µm thickness. Tissue sections were stained with hematoxylin and eosin (H&E) for morphology or Masson's Trichrome for fibrosis [83]. Images were acquired using a Keyence BZ-X810 microscope. Histopathological scores were blindly assessed as described previously.[85] Briefly, each colon was assessed for four parameters: inflammatory cell infiltration, epithelial architecture destruction, crypt dilatation, and fibrosis within the mucosa, submucosa, and serosa. Significant histopathological features, such as loss of crypt structure, goblet cell depletion, mucosal erosion, and submucosal fibrosis were recorded to further distinguish the severity of colonic injury and inflammation.

Immunohistochemistry

For IHC, paraffin sections were deparaffinized and subjected to heat-induced antigen retrieval using sodium citrate buffer (10 mM sodium citrate, 0.05% Tween-20, pH 6.0) for 20 minutes. Sections were incubated overnight at 4°C with a rabbit anti-MUC2 antibody (Genetex, GTX100664) diluted in PBS containing 5% normal serum and 1% BSA. Detection was performed using Alexa Fluor 488-conjugated goat anti-rabbit secondary antibody (Thermo Fisher Scientific, A32731TR). Nuclei were counterstained with 4',6-diamidino-2-phenylindole (DAPI) and imaged using a Nikon A1R confocal microscope.

Fluorescence in-situ hybridization (FISH)

A BI-specific probe was designed according to established guidelines.[86] Following the reported nomenclature,[87] the probe was designated S-S-B.int-0461-a-S-22 and is referred to herein as "Bint461" for clarity and convenience. The probe was 5'-labeled with sulfonated fluorescein 488 (Sigma-Aldrich). To assess specificity, FISH was performed on pure cultures of BI and *Escherichia coli* as described.[88] Localization of BI in colon sections from mono-associated mice was assessed using the Bint461 probe. Total bacterial presence was simultaneously detected using a universal bacterial FISH probe, S-D-Bact-0338-a-A-18 (Eub338), 5'-labeled with Texas Red as a positive control.[89] The NONEUB338 probe, designed as the reverse complement of EUB338, was included as a negative control. Slides were counterstained with DAPI and images were acquired using a Nikon A1R confocal microscope. Probe sequences are provided in Table S10.

Ferulic acid measurements

Absolute quantification of ferulic acid was done using Liquid Chromatography-tandem Mass Spectrometry (LC-MS/MS) by the Carver Metabolomics Core Facility at UIUC. Briefly, serum samples were spiked with a mixture of deuterium- and stable isotope-labeled internal standards prior to alkaline hydrolysis with NaOH, which facilitated the release of ferulic acid from its conjugated forms. Total ferulic acid content, comprising both free ferulic acid and that liberated from conjugates, was subsequently quantified.

Untargeted metabolomics assay

Samples were spiked with isotope-labeled internal standards prior to extraction and processed for untargeted metabolomics by the Carver Metabolomics Core at the Roy J. Carver Biotechnology Center at UIUC. Fecal samples were normalized to input dry fecal weight. Metabolomic profiling was performed using a Dionex Ultimate 3000 UHPLC system coupled to a Q-Exactive mass spectrometer. Metabolites were separated by reversed-phase chromatography on a Waters Acquity BEH C18 column (100 × 2.1 mm, 1.7 µm) maintained at 30 °C with a flow rate of 0.3 mL/min, using a water/acetonitrile gradient containing 0.1% formic acid. Data were acquired in both positive and negative electrospray ionization modes. Raw LC–MS data were processed using MS-DIAL (v4.90) for feature detection, alignment, adduct annotation, and compound identification based on accurate mass, MS/MS spectra, and retention time matching to an in-house standards library and public databases (MoNA, MassBank, GNPS, METLIN, and NIST20). Features with a sample-to-blank ratio <10 were excluded, and metabolites were assigned confidence levels according to Metabolomics Standards Initiative (MSI) guidelines. Positive and negative ionization datasets were merged, duplicate features were removed using quality control metrics, and peak intensities were normalized to internal standards. Principal component analysis was used for data quality assessment and outlier detection.

Metabolomics Data Processing and Statistical Analysis

Pairwise comparisons between experimental groups were performed using a custom function that calculated log2 fold changes and p-values for each metabolite. Zero values were excluded prior to analysis. Metabolite intensities were compared between groups using t-tests assuming unequal variance. P-values were adjusted for multiple testing using the false discovery rate (FDR) method. Significant metabolites were defined based on both p-value (<0.05) and log2 fold change thresholds. Volcano plots were generated to highlight significant up- and down-regulated metabolites. Heatmaps of selected metabolites were created with row-standardization (Z-score) applied.

To investigate shared and unique metabolites across group comparisons, Venn diagrams and UpSet plots were constructed. Metabolites were classified as "unique" or "shared" based on their occurrence across comparisons, and compound class information was retrieved from external databases. Pie charts were generated to visualize the distribution of metabolite categories for up- and down-regulated metabolites across group comparisons.

All data processing, statistical analyses, and visualizations were performed in R (v4.5.1) using the following packages: ggplot2 (v4.0.1),[90] ggrepel (v0.9.6),[91] ComplexHeatmap (v2.16.0),[92] patchwork (v1.3.2),[93] dplyr (v1.1.4), tidyr (v1.3.1), tibble (v3.3.0), and readxl (v1.4.5).[90]

Targeted bile acid assay

Samples were analyzed using LC-MS by the Carver Metabolomics Core of the Roy J. Carver Biotechnology Center, UIUC. The bile acid standard solution (Cayman chemical, Ann Arbor, Michigan, USA), containing 1 mg/mL of each of targeted bile acids was used to create a calibration curve for quantification. At the beginning of the extraction process, surrogate internal standards were spiked into each sample. Instrument internal standards (CUDA, PUHA, 0.1 µg/mL) were included in the reconstitution solution. Chromatography was performed on an Agilent 1290 Infinity II UHPLC system, with Waters Acquity C18 BEH 2.1 x 100mm, 1.7um; flow rate 450 µL/min. Mobile phases: 0.1% formic acid in water (A), 0.1% formic acid in acetonitrile (B); column temperature 60°C. Data was collected on an Agilent 6495C triple quadrupole mass spectrometer. Data was acquired in negative mode MRM mode, with source gas flow of 20.0 L/min, nebulizer pressure of 25.0 psi, sheath gas flow of 11.0 L/min, capillary voltage of 5000 V, nozzle voltage of 1000 V, high pressure iFunnel RF of 200 V, and low pressure iFunnel RF of 160 V. Data was acquired in negative mode MRM mode. Peak integration and quantitation using calibration curves adjusted for internal standards were done using Mass Hunter Quant 12.1.

Significantly altered bile acids were identified using a two-tailed Mann–Whitney U test. A p-value < 0.05 was considered statistically significant.

RNA-sequencing analysis

RNAs were extracted from the colons and spleens using PureLink RNA Mini Kit (Thermo Fisher Scientific, 12183025). RNA-seq libraries were constructed and sequenced at the UIUC Biotechnology Center High-Throughput Sequencing Core. Each library generated over 80 million single-end reads.

Adaptor sequences and low-quality bases were removed from the raw sequencing data using Trimmomatic v0.39.[94] Transcript abundance was quantified using Kallisto v0.44.0,[95] aligning reads to the mouse transcriptome (GRCm39, Ensembl). Data quality and sample consistency were evaluated through principal component analysis (PCA) and hierarchical clustering based on transcript quantifications. Transcript-level expression values corresponding to the same gene were then aggregated to obtain gene-level expression estimates. Differentially expressed genes (DEGs) were identified using DESeq2 v2_1.46.0,[96] with a significance threshold of adjusted p-value < 0.05 and $|\log2 \text{ fold change}| > 1$. Gene Ontology (GO) functional enrichment analysis was performed using Metascape identify significantly enriched biological processes, molecular functions, and cellular components.[97]

Immune Cell Fraction Analysis

Immune cell composition was assessed from bulk RNA-seq data using a deconvolution-based approach implemented in the R package immunedeconv.[98] Mouse gene symbols were converted to their human orthologs using the convert-human-mouse-genes function. Immune cell fractions were inferred using quanTIseq,[99] a constrained least squares regression method, with all expressed genes (TPM as the unit) to deconvolute the relative proportions of immune cell populations within each sample.

Quantitative Real-Time PCR (qPCR)

RNAs were extracted using TRIzol reagent according to standard protocols. Real-time PCR reactions were performed blindly in duplicate using the SYBR green master mix. Primer sequences are shown in Table S10.

Statistical analysis

Graphs were generated using R or GraphPad Prism software. Data normality in body weight, intestine length, goblet cell proportion, and mucus layer thickness was assessed using the Shapiro-Wilk test. Statistical significance between experimental and control groups was determined using a two-tailed unpaired Student's *t*-test or a two-tailed Mann-Whitney U test, unless otherwise specified.

Data availability

All raw RNA-seq data files are available for download from the Gene Expression Omnibus (accession number GSE318341).

ACKNOWLEDGMENTS

We thank Dr. Bo Wang, Ms. Tiantian Yang, and Mr. Zhiming Zhao for technical assistance with metabolic parameter measurements, Dr. Kun Wang for suggestions on immune cell fraction analysis, and Dr. Nicole Koropatkin (University of Michigan) for advice on testing BI function. We thank Dr. Alexander Ulanov, Dr. Michael Frano, and Ms. Wei Lu at the Metabolomics Core of the Roy J. Carver Biotechnology Center, UIUC, for assistance with metabolomics data processing. Karen Doty at the Histology Laboratory for assistance with histological staining.

FUNDING

This work was supported by the National Institutes of Health (R01 GM140306 to W.M. and I.C.; R01 ES036194 to W.M. and J.Y.; and R01 GM131810 to J.Y.), the UIUC Campus Research Board funds (RB25121 to W.M.), the UIUC Gnotobiotic Facility seed funds (to W.M.), the UIUC National Center for Supercomputing Applications Computes Program funds (to W.M.), and the UIUC Cancer Center at Illinois Jump Start funds (to W.M.).

CONFLICT OF INTEREST: The authors declare no conflict of interest.

DECLARATION OF GENERATIVE AI AND AI-ASSISTED TECHNOLOGIES IN THE MANUSCRIPT PREPARATION PROCESS

During the preparation of this work, the author(s) used ChatGPT in order to check spelling and grammar and improve English phrasing. After using this tool/service, the author(s) reviewed and edited the content as needed and take(s) full responsibility for the content of the published article.

References

1. Adolph, T.E., and Tilg, H. (2024). Western diets and chronic diseases. Nat Med *30*, 2133-2147. 10.1038/s41591-024-03165-6.
2. Makki, K., Deehan, E.C., Walter, J., and Backhed, F. (2018). The Impact of Dietary Fiber on Gut Microbiota in Host Health and Disease. Cell Host Microbe *23*, 705-715. 10.1016/j.chom.2018.05.012.
3. Khan, N.A., Raine, L.B., Drollette, E.S., Scudder, M.R., Kramer, A.F., and Hillman, C.H. (2015). Dietary fiber is positively associated with cognitive control among prepubertal children. J Nutr *145*, 143-149. 10.3945/jn.114.198457.
4. Prokopidis, K., Giannos, P., Ispoglou, T., Witard, O.C., and Isanejad, M. (2022). Dietary Fiber Intake is Associated with Cognitive Function in Older Adults: Data from the National Health and Nutrition Examination Survey. Am J Med *135*, e257-e262. 10.1016/j.amjmed.2022.03.022.
5. Liu, X.F., Shao, J.H., Liao, Y.T., Wang, L.N., Jia, Y., Dong, P.J., Liu, Z.Z., He, D.D., Li, C., and Zhang, X. (2023). Regulation of short-chain fatty acids in the immune system. Front Immunol *14*, 1186892. 10.3389/fimmu.2023.1186892.
6. Liu, P., Wang, Y., Yang, G., Zhang, Q., Meng, L., Xin, Y., and Jiang, X. (2021). The role of short-chain fatty acids in intestinal barrier function, inflammation, oxidative stress, and colonic carcinogenesis. Pharmacol Res *165*, 105420. 10.1016/j.phrs.2021.105420.
7. Munte, E., and Hartmann, P. (2025). The Role of Short-Chain Fatty Acids in Metabolic Dysfunction-Associated Steatotic Liver Disease and Other Metabolic Diseases. Biomolecules *15*. 10.3390/biom15040469.
8. Silva, Y.P., Bernardi, A., and Frozza, R.L. (2020). The Role of Short-Chain Fatty Acids From Gut Microbiota in Gut-Brain Communication. Front Endocrinol (Lausanne) *11*, 25. 10.3389/fendo.2020.00025.
9. Grant, E.T., De Franco, H., and Desai, M.S. (2025). Non-SCFA microbial metabolites associated with fiber fermentation and host health. Trends Endocrinol Metab *36*, 70-82. 10.1016/j.tem.2024.06.009.
10. Bakir, M.A., Kitahara, M., Sakamoto, M., Matsumoto, M., and Benno, Y. (2006). Bacteroides intestinalis sp. nov., isolated from human faeces. Int J Syst Evol Microbiol *56*, 151-154. 10.1099/ijs.0.63914-0.
11. Pereira, G.V., Abdel-Hamid, A.M., Dutta, S., D'Alessandro-Gabazza, C.N., Wefers, D., Farris, J.A., Bajaj, S., Wawrzak, Z., Atomi, H., Mackie, R.I., et al. (2021). Degradation of complex arabinoxylans by human colonic Bacteroidetes. Nat Commun *12*, 459. 10.1038/s41467-020-20737-5.
12. P, N.P.V., and Joye, I.J. (2020). Dietary Fibre from Whole Grains and Their Benefits on Metabolic Health. Nutrients *12*. 10.3390/nu12103045.
13. Chen, Z., Mense, A.L., Brewer, L.R., and Shi, Y.C. (2024). Wheat bran arabinoxylans: Chemical structure, extraction, properties, health benefits, and uses in foods. Compr Rev Food Sci Food Saf *23*, e13366. 10.1111/1541-4337.13366.
14. Ozcan, U., Yilmaz, E., Ozcan, L., Furuhashi, M., Vaillancourt, E., Smith, R.O., Gorgun, C.Z., and Hotamisligil, G.S. (2006). Chemical chaperones reduce ER stress and restore glucose homeostasis in a mouse model of type 2 diabetes. Science *313*, 1137-1140. 10.1126/science.1128294.
15. Kars, M., Yang, L., Gregor, M.F., Mohammed, B.S., Pietka, T.A., Finck, B.N., Patterson, B.W., Horton, J.D., Mittendorfer, B., Hotamisligil, G.S., and Klein, S. (2010).

Tauroursodeoxycholic Acid may improve liver and muscle but not adipose tissue insulin sensitivity in obese men and women. Diabetes *59*, 1899-1905. 10.2337/db10-0308.
16. Zheng, X., Chen, T., Jiang, R., Zhao, A., Wu, Q., Kuang, J., Sun, D., Ren, Z., Li, M., Zhao, M., et al. (2021). Hyocholic acid species improve glucose homeostasis through a distinct TGR5 and FXR signaling mechanism. Cell Metab *33*, 791-803 e797. 10.1016/j.cmet.2020.11.017.
17. Fagiolini, A., Cardoner, N., Pirildar, S., Ittsakul, P., Ng, B., Duailibi, K., and El Hindy, N. (2023). Moving from serotonin to serotonin-norepinephrine enhancement with increasing venlafaxine dose: clinical implications and strategies for a successful outcome in major depressive disorder. Expert Opin Pharmacother *24*, 1715-1723. 10.1080/14656566.2023.2242264.
18. Cefalu, A.B., Spina, R., Noto, D., Valenti, V., Ingrassia, V., Giammanco, A., Panno, M.D., Ganci, A., Barbagallo, C.M., and Averna, M.R. (2015). Novel CREB3L3 Nonsense Mutation in a Family With Dominant Hypertriglyceridemia. Arterioscler Thromb Vasc Biol *35*, 2694-2699. 10.1161/ATVBAHA.115.306170.
19. Dron, J.S., Dilliott, A.A., Lawson, A., McIntyre, A.D., Davis, B.D., Wang, J., Cao, H., Movsesyan, I., Malloy, M.J., Pullinger, C.R., et al. (2020). Loss-of-Function CREB3L3 Variants in Patients With Severe Hypertriglyceridemia. Arterioscler Thromb Vasc Biol *40*, 1935-1941. 10.1161/ATVBAHA.120.314168.
20. Gurevitz, C., Mechanick, J.I., Do, R., and Rosenson, R.S. (2025). Hypertriglyceridemia-induced acute pancreatitis in pregnancy associated with CREB3L3 mutation. J Clin Lipidol *19*, 173-177. 10.1016/j.jacl.2024.10.001.
21. Nakagawa, Y., Satoh, A., Tezuka, H., Han, S.I., Takei, K., Iwasaki, H., Yatoh, S., Yahagi, N., Suzuki, H., Iwasaki, Y., et al. (2016). CREB3L3 controls fatty acid oxidation and ketogenesis in synergy with PPARalpha. Sci Rep *6*, 39182. 10.1038/srep39182.
22. Siepka, S.M., Yoo, S.H., Park, J., Song, W., Kumar, V., Hu, Y., Lee, C., and Takahashi, J.S. (2007). Circadian mutant Overtime reveals F-box protein FBXL3 regulation of cryptochrome and period gene expression. Cell *129*, 1011-1023. 10.1016/j.cell.2007.04.030.
23. Goriki, A., Hatanaka, F., Myung, J., Kim, J.K., Yoritaka, T., Tanoue, S., Abe, T., Kiyonari, H., Fujimoto, K., Kato, Y., et al. (2014). A novel protein, CHRONO, functions as a core component of the mammalian circadian clock. PLoS Biol *12*, e1001839. 10.1371/journal.pbio.1001839.
24. Gachon, F. (2007). Physiological function of PARbZip circadian clock-controlled transcription factors. Ann Med *39*, 562-571. 10.1080/07853890701491034.
25. Campbell, N.K., Fitzgerald, H.K., and Dunne, A. (2021). Regulation of inflammation by the antioxidant haem oxygenase 1. Nat Rev Immunol *21*, 411-425. 10.1038/s41577-020-00491-x.
26. Zannas, A.S., Wiechmann, T., Gassen, N.C., and Binder, E.B. (2016). Gene-Stress-Epigenetic Regulation of FKBP5: Clinical and Translational Implications. Neuropsychopharmacology *41*, 261-274. 10.1038/npp.2015.235.
27. Ravenna, L., Salvatori, L., and Russo, M.A. (2016). HIF3alpha: the little we know. FEBS J *283*, 993-1003. 10.1111/febs.13572.
28. Barone, S., Fussell, S.L., Singh, A.K., Lucas, F., Xu, J., Kim, C., Wu, X., Yu, Y., Amlal, H., Seidler, U., et al. (2009). Slc2a5 (Glut5) is essential for the absorption of fructose in

the intestine and generation of fructose-induced hypertension. J Biol Chem *284*, 5056-5066. 10.1074/jbc.M808128200.
29. Horsey, A.J., Cox, M.H., Sarwat, S., and Kerr, I.D. (2016). The multidrug transporter ABCG2: still more questions than answers. Biochem Soc Trans *44*, 824-830. 10.1042/BST20160014.
30. Istiaq, A., and Ohta, K. (2022). A review on Tsukushi: mammalian development, disorders, and therapy. J Cell Commun Signal *16*, 505-513. 10.1007/s12079-022-00669-z.
31. Tabibzadeh, S., and Hemmati-Brivanlou, A. (2006). Lefty at the crossroads of "stemness" and differentiative events. Stem Cells *24*, 1998-2006. 10.1634/stemcells.2006-0075.
32. Nassel, D.R., Zandawala, M., Kawada, T., and Satake, H. (2019). Tachykinins: Neuropeptides That Are Ancient, Diverse, Widespread and Functionally Pleiotropic. Front Neurosci *13*, 1262. 10.3389/fnins.2019.01262.
33. Shindo, R., Katagiri, T., Komazawa-Sakon, S., Ohmuraya, M., Takeda, W., Nakagawa, Y., Nakagata, N., Sakuma, T., Yamamoto, T., Nishiyama, C., et al. (2020). Regenerating islet-derived protein (Reg)3beta plays a crucial role in attenuation of ileitis and colitis in mice. Biochem Biophys Rep *21*, 100738. 10.1016/j.bbrep.2020.100738.
34. van Ampting, M.T., Loonen, L.M., Schonewille, A.J., Konings, I., Vink, C., Iovanna, J., Chamaillard, M., Dekker, J., van der Meer, R., Wells, J.M., and Bovee-Oudenhoven, I.M. (2012). Intestinally secreted C-type lectin Reg3b attenuates salmonellosis but not listeriosis in mice. Infect Immun *80*, 1115-1120. 10.1128/IAI.06165-11.
35. Wang, L., Fouts, D.E., Starkel, P., Hartmann, P., Chen, P., Llorente, C., DePew, J., Moncera, K., Ho, S.B., Brenner, D.A., et al. (2016). Intestinal REG3 Lectins Protect against Alcoholic Steatohepatitis by Reducing Mucosa-Associated Microbiota and Preventing Bacterial Translocation. Cell Host Microbe *19*, 227-239. 10.1016/j.chom.2016.01.003.
36. Shrestha, N., Bahnan, W., Wiley, D.J., Barber, G., Fields, K.A., and Schesser, K. (2012). Eukaryotic initiation factor 2 (eIF2) signaling regulates proinflammatory cytokine expression and bacterial invasion. J Biol Chem *287*, 28738-28744. 10.1074/jbc.M112.375915.
37. Ku, Y.C., Lai, M.H., Lo, C.C., Cheng, Y.C., Qiu, J.T., Tarn, W.Y., and Lai, M.C. (2019). DDX3 Participates in Translational Control of Inflammation Induced by Infections and Injuries. Mol Cell Biol *39*. 10.1128/MCB.00285-18.
38. Cunningham, C.M., Li, M., Ruffenach, G., Doshi, M., Aryan, L., Hong, J., Park, J., Hrncir, H., Medzikovic, L., Umar, S., et al. (2022). Y-Chromosome Gene, Uty, Protects Against Pulmonary Hypertension by Reducing Proinflammatory Chemokines. Am J Respir Crit Care Med *206*, 186-196. 10.1164/rccm.202110-2309OC.
39. Chen, J., Wang, T., Zhang, D., Wang, H., Huang, Z., Yang, Z., Li, J., Hu, T., Wang, X., and Li, X. (2024). KDM5D histone demethylase mediates p38alpha inactivation via its enzymatic activity to inhibit cancer progression. Proc Natl Acad Sci U S A *121*, e2402022121. 10.1073/pnas.2402022121.
40. Bresciani, E., Broadbridge, E., and Liu, P.P. (2018). An efficient dissociation protocol for generation of single cell suspension from zebrafish embryos and larvae. MethodsX *5*, 1287-1290. 10.1016/j.mex.2018.10.009.
41. Kawano, N., Araki, N., Yoshida, K., Hibino, T., Ohnami, N., Makino, M., Kanai, S., Hasuwa, H., Yoshida, M., Miyado, K., and Umezawa, A. (2014). Seminal vesicle protein

SVS2 is required for sperm survival in the uterus. Proc Natl Acad Sci U S A *111*, 4145-4150. 10.1073/pnas.1320715111.
42. Mendoza, A., Tang, C., Choi, J., Acuna, M., Logan, M., Martin, A.G., Al-Sowaimel, L., Desai, B.N., Tenen, D.E., Jacobs, C., et al. (2021). Thyroid hormone signaling promotes hepatic lipogenesis through the transcription factor ChREBP. Sci Signal *14*, eabh3839. 10.1126/scisignal.abh3839.
43. Flowers, M.T., and Ntambi, J.M. (2008). Role of stearoyl-coenzyme A desaturase in regulating lipid metabolism. Curr Opin Lipidol *19*, 248-256. 10.1097/MOL.0b013e3282f9b54d.
44. Chandrasekaran, P., Weiskirchen, S., and Weiskirchen, R. (2024). Perilipins: A family of five fat-droplet storing proteins that play a significant role in fat homeostasis. J Cell Biochem *125*, e30579. 10.1002/jcb.30579.
45. Kei, A.A., Filippatos, T.D., Tsimihodimos, V., and Elisaf, M.S. (2012). A review of the role of apolipoprotein C-II in lipoprotein metabolism and cardiovascular disease. Metabolism *61*, 906-921. 10.1016/j.metabol.2011.12.002.
46. Kersten, S. (2021). Role and mechanism of the action of angiopoietin-like protein ANGPTL4 in plasma lipid metabolism. J Lipid Res *62*, 100150. 10.1016/j.jlr.2021.100150.
47. Lian, J., Nelson, R., and Lehner, R. (2018). Carboxylesterases in lipid metabolism: from mouse to human. Protein Cell *9*, 178-195. 10.1007/s13238-017-0437-z.
48. Mouchiroud, M., Camire, E., Aldow, M., Caron, A., Jubinville, E., Turcotte, L., Kaci, I., Beaulieu, M.J., Roy, C., Labbe, S.M., et al. (2019). The hepatokine Tsukushi is released in response to NAFLD and impacts cholesterol homeostasis. JCI Insight *4*. 10.1172/jci.insight.129492.
49. Chen, C., Shah, Y.M., Morimura, K., Krausz, K.W., Miyazaki, M., Richardson, T.A., Morgan, E.T., Ntambi, J.M., Idle, J.R., and Gonzalez, F.J. (2008). Metabolomics reveals that hepatic stearoyl-CoA desaturase 1 downregulation exacerbates inflammation and acute colitis. Cell Metab *7*, 135-147. 10.1016/j.cmet.2007.12.003.
50. Pallotta, M.T., Rossini, S., Suvieri, C., Coletti, A., Orabona, C., Macchiarulo, A., Volpi, C., and Grohmann, U. (2022). Indoleamine 2,3-dioxygenase 1 (IDO1): an up-to-date overview of an eclectic immunoregulatory enzyme. FEBS J *289*, 6099-6118. 10.1111/febs.16086.
51. Kenney, L.L., Chiu, R.S., Dutra, M.N., Wactor, A., Honan, C., Shelerud, L., Corrigan, J.J., Yu, K., Ferrari, J.D., Jeffrey, K.L., et al. (2024). mRNA-delivery of IDO1 suppresses T cell-mediated autoimmunity. Cell Rep Med *5*, 101717. 10.1016/j.xcrm.2024.101717.
52. Gao, Z., Shao, S., Xu, Z., Nie, J., Li, C., and Du, C. (2025). IDO1 induced macrophage M1 polarization via ER stress-associated GRP78-XBP1 pathway to promote ulcerative colitis progression. Front Med (Lausanne) *12*, 1524952. 10.3389/fmed.2025.1524952.
53. Pejler, G., Ronnberg, E., Waern, I., and Wernersson, S. (2010). Mast cell proteases: multifaceted regulators of inflammatory disease. Blood *115*, 4981-4990. 10.1182/blood-2010-01-257287.
54. Button, J.E., Autran, C.A., Reens, A.L., Cosetta, C.M., Smriga, S., Ericson, M., Pierce, J.V., Cook, D.N., Lee, M.L., Sun, A.K., et al. (2022). Dosing a synbiotic of human milk oligosaccharides and B. infantis leads to reversible engraftment in healthy adult microbiomes without antibiotics. Cell Host Microbe *30*, 712-725 e717. 10.1016/j.chom.2022.04.001.

55. Asosingh, K., Lauruschkat, C.D., Alemagno, M., Frimel, M., Wanner, N., Weiss, K., Kessler, S., Meyers, D.A., Bennett, C., Xu, W., and Erzurum, S. (2020). Arginine metabolic control of airway inflammation. JCI Insight *5*. 10.1172/jci.insight.127801.
56. De Santi, C., Nally, F.K., Afzal, R., Duffy, C.P., Fitzsimons, S., Annett, S.L., Robson, T., Dowling, J.K., Cryan, S.A., and McCoy, C.E. (2022). Enhancing arginase 2 expression using target site blockers as a strategy to modulate macrophage phenotype. Mol Ther Nucleic Acids *29*, 643-655. 10.1016/j.omtn.2022.08.004.
57. Dowling, J.K., Afzal, R., Gearing, L.J., Cervantes-Silva, M.P., Annett, S., Davis, G.M., De Santi, C., Assmann, N., Dettmer, K., Gough, D.J., et al. (2021). Mitochondrial arginase-2 is essential for IL-10 metabolic reprogramming of inflammatory macrophages. Nat Commun *12*, 1460. 10.1038/s41467-021-21617-2.
58. Millet, V., Gensollen, T., Maltese, M., Serrero, M., Lesavre, N., Bourges, C., Pitaval, C., Cadra, S., Chasson, L., Vu Man, T.P., et al. (2023). Harnessing the Vnn1 pantetheinase pathway boosts short chain fatty acids production and mucosal protection in colitis. Gut *72*, 1115-1128. 10.1136/gutjnl-2021-325792.
59. Li, J., and Dawson, P.A. (2019). Animal models to study bile acid metabolism. Biochim Biophys Acta Mol Basis Dis *1865*, 895-911. 10.1016/j.bbadis.2018.05.011.
60. Eyssen, H.J., De Pauw, G., and Van Eldere, J. (1999). Formation of hyodeoxycholic acid from muricholic acid and hyocholic acid by an unidentified gram-positive rod termed HDCA-1 isolated from rat intestinal microflora. Appl Environ Microbiol *65*, 3158-3163. 10.1128/AEM.65.7.3158-3163.1999.
61. Zheng, X., Chen, T., Zhao, A., Ning, Z., Kuang, J., Wang, S., You, Y., Bao, Y., Ma, X., Yu, H., et al. (2021). Hyocholic acid species as novel biomarkers for metabolic disorders. Nat Commun *12*, 1487. 10.1038/s41467-021-21744-w.
62. Kuang, J., Wang, J., Li, Y., Li, M., Zhao, M., Ge, K., Zheng, D., Cheung, K.C.P., Liao, B., Wang, S., et al. (2023). Hyodeoxycholic acid alleviates non-alcoholic fatty liver disease through modulating the gut-liver axis. Cell Metab *35*, 1752-1766 e1758. 10.1016/j.cmet.2023.07.011.
63. Sehayek, E., Ono, J.G., Duncan, E.M., Batta, A.K., Salen, G., Shefer, S., Neguyen, L.B., Yang, K., Lipkin, M., and Breslow, J.L. (2001). Hyodeoxycholic acid efficiently suppresses atherosclerosis formation and plasma cholesterol levels in mice. J Lipid Res *42*, 1250-1256.
64. Zhong, J., He, X., Gao, X., Liu, Q., Zhao, Y., Hong, Y., Zhu, W., Yan, J., Li, Y., Li, Y., et al. (2023). Hyodeoxycholic acid ameliorates nonalcoholic fatty liver disease by inhibiting RAN-mediated PPARalpha nucleus-cytoplasm shuttling. Nat Commun *14*, 5451. 10.1038/s41467-023-41061-8.
65. Cohen-Solal, C., Parquet, M., Ferezou, J., Serougne, C., and Lutton, C. (1995). Effects of hyodeoxycholic acid and alpha-hyocholic acid, two 6 alpha-hydroxylated bile acids, on cholesterol and bile acid metabolism in the hamster. Biochim Biophys Acta *1257*, 189-197. 10.1016/0005-2760(95)00073-l.
66. Shih, D.M., Shaposhnik, Z., Meng, Y., Rosales, M., Wang, X., Wu, J., Ratiner, B., Zadini, F., Zadini, G., and Lusis, A.J. (2013). Hyodeoxycholic acid improves HDL function and inhibits atherosclerotic lesion formation in LDLR-knockout mice. FASEB J *27*, 3805-3817. 10.1096/fj.12-223008.
67. Oluwole, O., Fernando, W.B., Lumanlan, J., Ademuyiwa, O., and Jayasena, V. (2022). Role of phenolic acid, tannins, stilbenes, lignans and flavonoids in human health – a

review. International Journal of Food Science and Technology *57*, 6326-6335. 10.1111/ijfs.15936.
68. Zhang, Y., Cai, P., Cheng, G., and Zhang, Y. (2022). A Brief Review of Phenolic Compounds Identified from Plants: Their Extraction, Analysis, and Biological Activity. Natural Product Communications *17*, 1934578X211069721. 10.1177/1934578x211069721.
69. Landete, J.M. (2012). Plant and mammalian lignans: A review of source, intake, metabolism, intestinal bacteria and health. Food Research International *46*, 410-424.
70. Heinonen, S., Nurmi, T., Liukkonen, K., Poutanen, K., Wahala, K., Deyama, T., Nishibe, S., and Adlercreutz, H. (2001). In vitro metabolism of plant lignans: new precursors of mammalian lignans enterolactone and enterodiol. J Agric Food Chem *49*, 3178-3186. 10.1021/jf010038a.
71. Amaral, J.D., Viana, R.J., Ramalho, R.M., Steer, C.J., and Rodrigues, C.M. (2009). Bile acids: regulation of apoptosis by ursodeoxycholic acid. J Lipid Res *50*, 1721-1734. 10.1194/jlr.R900011-JLR200.
72. Engin, F., Yermalovich, A., Nguyen, T., Hummasti, S., Fu, W., Eizirik, D.L., Mathis, D., and Hotamisligil, G.S. (2013). Restoration of the unfolded protein response in pancreatic beta cells protects mice against type 1 diabetes. Sci Transl Med *5*, 211ra156. 10.1126/scitranslmed.3006534.
73. Bronczek, G.A., Vettorazzi, J.F., Soares, G.M., Kurauti, M.A., Santos, C., Bonfim, M.F., Carneiro, E.M., Balbo, S.L., Boschero, A.C., and Costa Junior, J.M. (2019). The Bile Acid TUDCA Improves Beta-Cell Mass and Reduces Insulin Degradation in Mice With Early-Stage of Type-1 Diabetes. Front Physiol *10*, 561. 10.3389/fphys.2019.00561.
74. Ochiai, T., Nagayama, T., Matsui, K., Amano, K., Sano, T., Wakabayashi, T., and Iwatsubo, T. (2021). Tauroursodeoxycholic Acid Attenuates Diet-Induced and Age-Related Peripheral Endoplasmic Reticulum Stress and Cerebral Amyloid Pathology in a Mouse Model of Alzheimer's Disease. J Prev Alzheimers Dis *8*, 483-494. 10.14283/jpad.2021.33.
75. Kusaczuk, M. (2019). Tauroursodeoxycholate-Bile Acid with Chaperoning Activity: Molecular and Cellular Effects and Therapeutic Perspectives. Cells *8*. 10.3390/cells8121471.
76. Si, Z.L., Wang, H.Y., Wang, T., Cao, Y.Z., Li, Q.Z., Liu, K., Huang, Z., Liu, H.L., Tan, Y.J., Wang, Y.Y., et al. (2024). Gut Bacteroides ovatus ameliorates renal fibrosis by promoting the production of HDCA through upregulation of Clostridium scindens. Cell Rep *43*, 114830. 10.1016/j.celrep.2024.114830.
77. Kyoko, O.O., Kono, H., Ishimaru, K., Miyake, K., Kubota, T., Ogawa, H., Okumura, K., Shibata, S., and Nakao, A. (2014). Expressions of tight junction proteins Occludin and Claudin-1 are under the circadian control in the mouse large intestine: implications in intestinal permeability and susceptibility to colitis. PLoS One *9*, e98016. 10.1371/journal.pone.0098016.
78. Nagao, Y., Taguchi, A., and Ohta, Y. (2025). Circadian Rhythm Dysregulation in Inflammatory Bowel Disease: Mechanisms and Chronotherapeutic Approaches. Int J Mol Sci *26*. 10.3390/ijms26083724.
79. Liu, X., Yu, R., Zhu, L., Hou, X., and Zou, K. (2017). Bidirectional Regulation of Circadian Disturbance and Inflammation in Inflammatory Bowel Disease. Inflamm Bowel Dis *23*, 1741-1751. 10.1097/MIB.0000000000001265.

80. Ye, Y., Liu, C., Wu, R., Kang, D., Gao, H., Lv, H., Feng, Z., Shi, Y., Liu, Z., and Chen, L. (2024). Circadian clock component PER2 negatively regulates CD4(+) T cell IFN-gamma production in ulcerative colitis. Mucosal Immunol *17*, 1161-1173. 10.1016/j.mucimm.2024.07.010.
81. Pagel, R., Bar, F., Schroder, T., Sunderhauf, A., Kunstner, A., Ibrahim, S.M., Autenrieth, S.E., Kalies, K., Konig, P., Tsang, A.H., et al. (2017). Circadian rhythm disruption impairs tissue homeostasis and exacerbates chronic inflammation in the intestine. FASEB J *31*, 4707-4719. 10.1096/fj.201700141RR.
82. Bacic, M.K., and Smith, C.J. (2008). Laboratory maintenance and cultivation of bacteroides species. Curr Protoc Microbiol *Chapter 13*, Unit 13C 11. 10.1002/9780471729259.mc13c01s9.
83. Sheehan, D.C.a.H., B.B. (1980). Theory and practice of histotechnology (The CV Mosby Company).
84. Luna, L.G. (1968). Manual of histologic staining methods of the Armed Forces Institute of Pathology (McGraw-Hill Publications).
85. Erben, U., Loddenkemper, C., Doerfel, K., Spieckermann, S., Haller, D., Heimesaat, M.M., Zeitz, M., Siegmund, B., and Kuhl, A.A. (2014). A guide to histomorphological evaluation of intestinal inflammation in mouse models. Int J Clin Exp Pathol *7*, 4557-4576.
86. Hugenholtz, P., Tyson, G.W., and Blackall, L.L. (2002). Design and evaluation of 16S rRNA-targeted oligonucleotide probes for fluorescence in situ hybridization. Methods Mol Biol *179*, 29-42. 10.1385/1-59259-238-4:029.
87. Alm, E.W., Oerther, D.B., Larsen, N., Stahl, D.A., and Raskin, L. (1996). The oligonucleotide probe database. Appl Environ Microbiol *62*, 3557-3559. 10.1128/aem.62.10.3557-3559.1996.
88. Zoetendal, E.G., Ben-Amor, K., Harmsen, H.J., Schut, F., Akkermans, A.D., and de Vos, W.M. (2002). Quantification of uncultured Ruminococcus obeum-like bacteria in human fecal samples by fluorescent in situ hybridization and flow cytometry using 16S rRNA-targeted probes. Appl Environ Microbiol *68*, 4225-4232. 10.1128/AEM.68.9.4225-4232.2002.
89. Amann, R.I., Binder, B.J., Olson, R.J., Chisholm, S.W., Devereux, R., and Stahl, D.A. (1990). Combination of 16S rRNA-targeted oligonucleotide probes with flow cytometry for analyzing mixed microbial populations. Appl Environ Microbiol *56*, 1919-1925. 10.1128/aem.56.6.1919-1925.1990.
90. Wickham, H. (2016). ggplot2 Elegant Graphics for Data Analysis (Springer).
91. K, S. (2018). ggrepel: Automatically Position Non-Overlapping Text Labels with 'ggplot2'. R package version 0.9.6.9999.
92. Gu, Z., Eils, R., and Schlesner, M. (2016). Complex heatmaps reveal patterns and correlations in multidimensional genomic data. Bioinformatics *32*, 2847-2849. 10.1093/bioinformatics/btw313.
93. T, P. (2019). patchwork: The Composer of Plots. R package version 1.3.
94. Bolger, A.M., Lohse, M., and Usadel, B. (2014). Trimmomatic: a flexible trimmer for Illumina sequence data. Bioinformatics *30*, 2114-2120. 10.1093/bioinformatics/btu170.
95. Bray, N.L., Pimentel, H., Melsted, P., and Pachter, L. (2016). Near-optimal probabilistic RNA-seq quantification. Nat Biotechnol *34*, 525-527. 10.1038/nbt.3519.

96. Love, M.I., Huber, W., and Anders, S. (2014). Moderated estimation of fold change and dispersion for RNA-seq data with DESeq2. Genome Biol *15*, 550. 10.1186/s13059-014-0550-8.
97. Zhou, Y., Zhou, B., Pache, L., Chang, M., Khodabakhshi, A.H., Tanaseichuk, O., Benner, C., and Chanda, S.K. (2019). Metascape provides a biologist-oriented resource for the analysis of systems-level datasets. Nat Commun *10*, 1523. 10.1038/s41467-019-09234-6.
98. Sturm, G., Finotello, F., and List, M. (2020). Immunedeconv: An R Package for Unified Access to Computational Methods for Estimating Immune Cell Fractions from Bulk RNA-Sequencing Data. Methods Mol Biol *2120*, 223-232. 10.1007/978-1-0716-0327-7_16.
99. Finotello, F., Mayer, C., Plattner, C., Laschober, G., Rieder, D., Hackl, H., Krogsdam, A., Loncova, Z., Posch, W., Wilflingseder, D., et al. (2019). Molecular and pharmacological modulators of the tumor immune contexture revealed by deconvolution of RNA-seq data. Genome Med *11*, 34. 10.1186/s13073-019-0638-6.

Figure legends

Figure 1. BI mono-association reduces mouse cecum size and enhances intestinal mucus secretion

(A) Schematic of the experimental design and treatments for each mouse group. (B) Representative images of the small intestine, cecum, and colon from mice in each group, with the ratio of cecum size and weight to body weight quantification shown on the right. (C) Alcian blue staining shows increased number of goblet cells in the proximal and distal colons of BI-inoculated mice. Quantification is shown on right. (D) Alcian blue-BHG staining showing increased thickness of colon mucus layer (red arrows) in BI-inoculated mice relative to germ-free (GF) mice and HK-BI-inoculated mice. quantification is shown on the right. Scale bars, 50 µm. * $p < 0.05$; **** $p < 0.0001$.

Figure 2. **BI and inWAX increased beneficial bile acids and phenolic compounds.**

(A) Schematic of the experimental workflow and treatments for each mouse group. (B) Comparison of systemic levels of ferulic acid across 6 groups of mice. (C) Partial least squares discriminant analysis (PLS-DA) showing distinct circulating metabolite profiles induced by inWAX versus cellulose in BI mono-associated mice. (D) Volcano plot showing differentially abundant circulating metabolites in inWAX-fed mice relative to cellulose-fed mice; bile acids are highlighted in green and phenolic compounds in purple. (E) Heatmaps showing inWAX-induced increases in phenolic compounds and bile acids. (F) Comparison of the GSH/GSSG ratio. * $p < 0.05$, one-tailed T-test. (G) Heatmaps showing inWAX-induced reductions in lysophosphatidylcholines (LPCs) and carnitine derivatives.

Figure 3. BI and inWAX activates genes essential for circadian regulation and triglyceride metabolism in the colon

(A) The volcano plot showing differentially expressed gene in the colon of inWAX-fed mice relative to the cellulose-fed mice. Circadian regulators are highlighted in blue and *Creb3l3* in red. (B) Schematic illustrating the roles of upregulated circadian regulatory genes within the circadian clock network. (C) Quantitative RT-PCR validation of selected upregulated genes. Expression levels were normalized to *Gapdh*. Each symbol represents an individual mouse; bars indicate mean values. * $p < 0.05$.

Figure 4. BI and inWAX ameliorates DSS-induced colitis

(A) Experimental schematic showing dietary acclimation, BI inoculation, and DSS treatment. Germ-free mice were acclimated to customized diets for 5 days, inoculated with BI, and treated with or without DSS for an additional 5 days. Compared with the cellu;DSS+ group, mice in the inWAX;DSS+ group exhibited reduced body weight loss (B), decreased splenomegaly (C), and lower histopathological scores for inflammation, crypt dilation, and fibrosis (D). Masson's Trichrome staining (blue in D) marks fibrosis. Bars represent 50 µm.

Figure 5. BI and inWAX remodels the colonic transcriptome in response to DSS.

(A) Volcano plot showing differentially expressed genes in the colons of inWAX-fed mice relative to cellulose-fed mice following DSS treatment. Y chromosome-linked genes are circled in blue and *Reg3b* is circled in red. (B) Gene Ontology (GO) analysis showing enrichment of lipid metabolism pathways among upregulated genes. (C) Heatmap showing upregulated metabolic

genes. (D) GO analysis showing enrichment of wound-healing pathways among downregulated genes.

Figure 6. BI and inWAX reshape the spleen immune cell landscape in response to DSS.
(A) H&E-stained spleen sections showing enlarged white pulp regions in inWAX-treated mice (arrows). (B) GO analysis showing enrichment of lymphocyte expansion and adaptive immune response pathways among genes upregulated by BI-inWAX. (C) GO analysis showing enrichment of cell division pathways among downregulated genes. (D) Stacked bar plot showing relative proportions of splenic immune cell lineages. (E) Bar plots showing statistically significant differences in immune cell proportions between inWAX- and cellulose-treated mice. (F) Heatmap showing genes upregulated in both the colon and spleen, including Y-linked and metabolic genes.

Figure 7. BI and inWAX improves glucose tolerance and bile acid profiles in HFD-induced obesity
(A) Schematic of the experimental workflow illustrating BI- and inWAX-based interventions in HFD-induced obese mice. All mice were inoculated with BI. (B) Glucose tolerance test results showing improved glucose clearance in inWAX-treated mice relative to HFD controls. (C) Comparison of bile acid concentrations and proportions showing BI and inWAX enhance the production of HCA, HDCA, and DCA. (D) Comparison of the ratios of HDCA to αMCA and βMCA as well as HDCA to HCA. (E) Comparison of the ratios of unconjugated to total bile acids showing increased deconjugation activities induced by inWAX and cellulose. * $p < 0.05$. ns, not significant.

Figure 8. BI and inWAX rewire gut metabolic outputs under HFD conditions
(A) Principal component analysis showing BI-inWAX induced a metabolite profile distinct from cellulose. (B) The UpSet plot showing metabolites uniquely or commonly altered among the indicated groups. (C) Pie chart showing structural classification of metabolites uniquely induced by BI-inWAX. (D) Heatmap showing increased production of neurotransmitters and their precursors. (E) Heatmap showing BI-inWAX-induced increases in microbial fermentation-derived bioactive phenolic compounds and vitamins, alongside reduced levels of plant-derived polyphenols. (F) Heatmap showing BI-inWAX downregulated phosphatidylcholine derivatives.

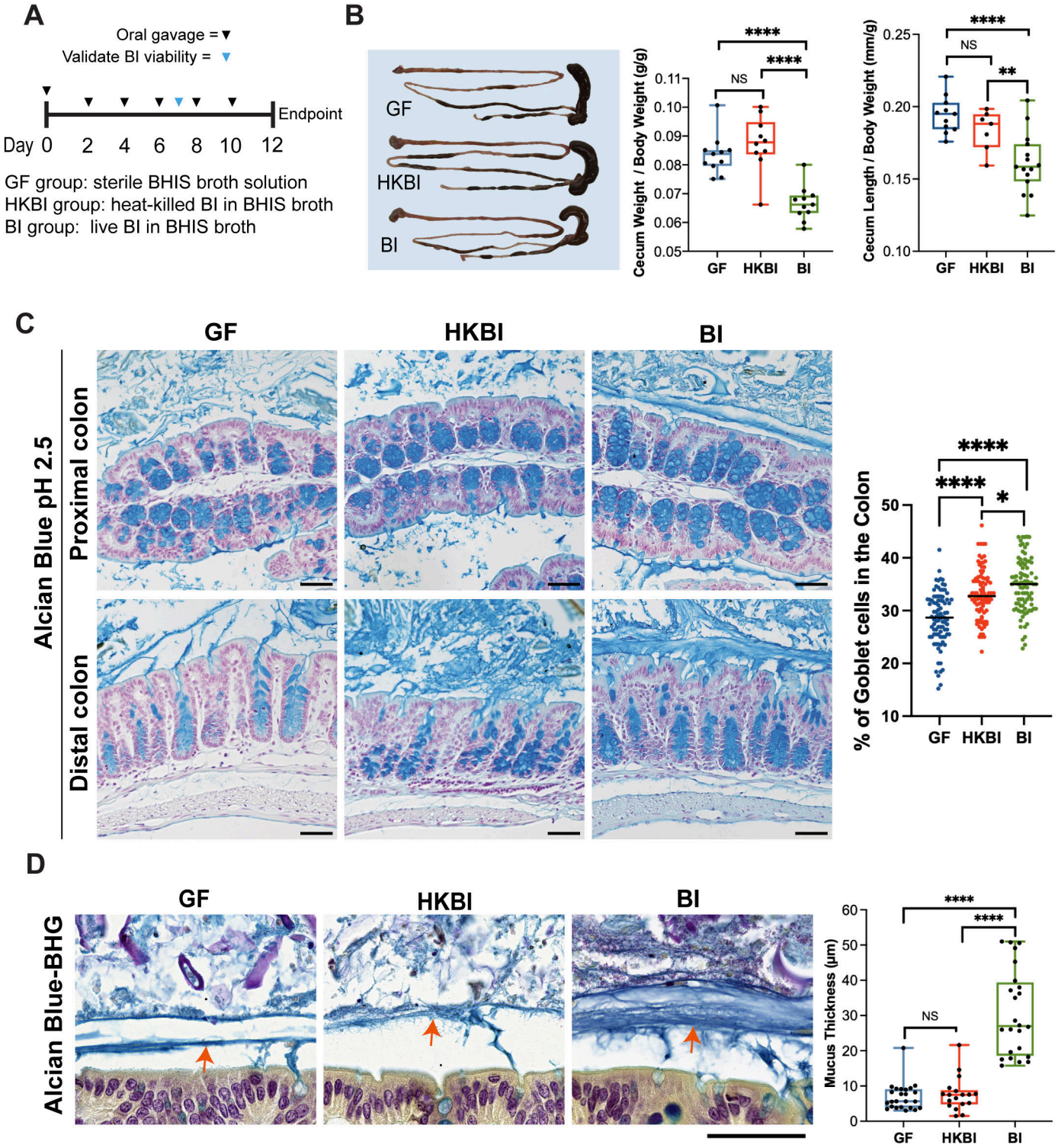
A
Oral gavage =
Validate BI viability =
Endpoint
Day 0 2 4 6 8 10 12
GF group: sterile BHIS broth solution
HKBI group: heat-killed BI in BHIS broth
BI group: live BI in BHIS broth
B
GF
HKBI
BI
Cecum Weight / Body Weight (g/g)
NS
****
****
Cecum Length / Body Weight (mm/g)
NS
****
**
C
GF
HKBI
BI
Alcian Blue pH 2.5
Proximal colon
Distal colon
% of Goblet cells in the Colon
****
****
*
D
GF
HKBI
BI
Alcian Blue-BHG
Mucus Thickness (µm)
NS
****
****

Figure 1

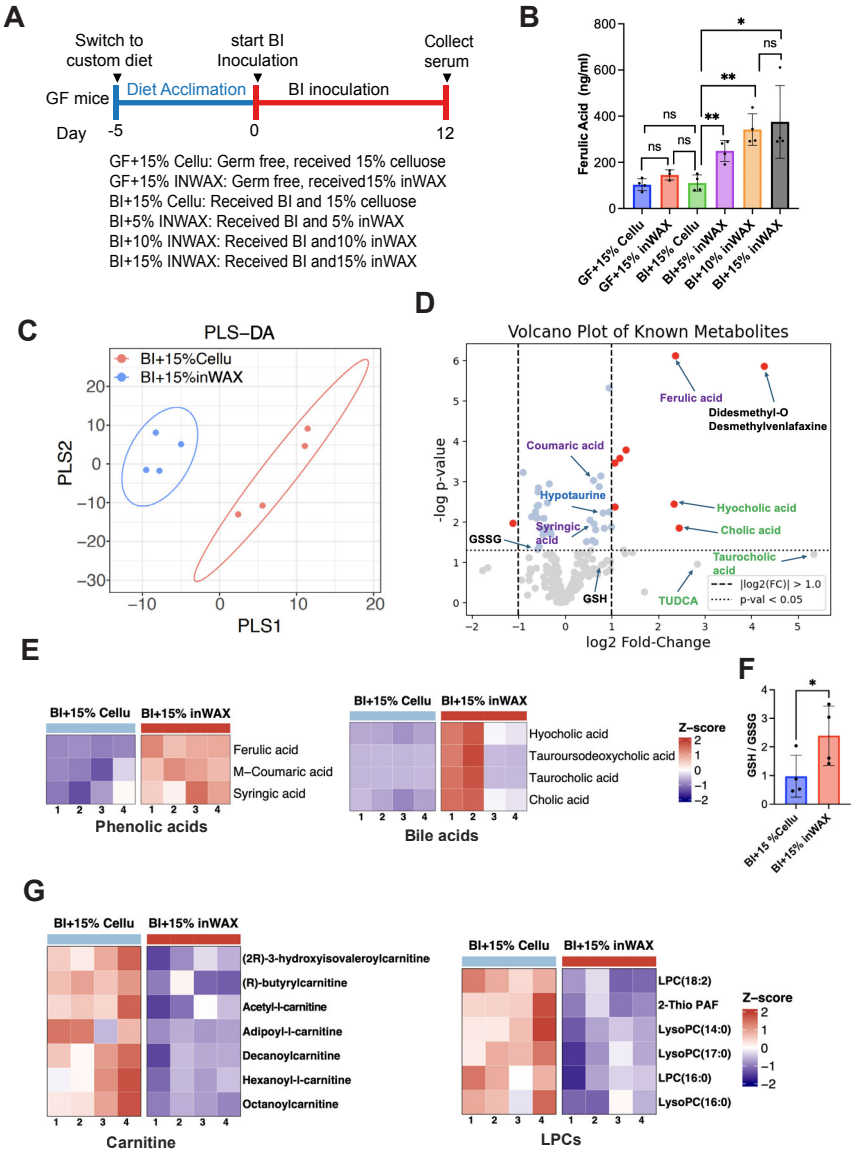
A
Switch to custom diet
start BI Inoculation
Collect serum
GF mice
Diet Acclimation
BI inoculation
Day
-5
0
12
GF+15% Cellu: Germ free, received 15% celluose
GF+15% INWAX: Germ free, received15% inWAX
BI+15% Cellu: Received BI and 15% celluose
BI+5% INWAX: Received BI and 5% inWAX
BI+10% INWAX: Received BI and10% inWAX
BI+15% INWAX: Received BI and15% inWAX
B
Ferulic Acid (ng/ml)
GF+15% Cellu
GF+15% inWAX
BI+15% Cellu
BI+5% inWAX
BI+10% inWAX
BI+15% inWAX
C
PLS–DA
BI+15%Cellu
BI+15%inWAX
PLS2
PLS1
D
Volcano Plot of Known Metabolites
-log p-value
log2 Fold-Change
Ferulic acid
Didesmethyl-O Desmethylvenlafaxine
Coumaric acid
Hypotaurine
Syringic acid
GSSG
GSH
Hyocholic acid
Cholic acid
Taurocholic acid
TUDCA
|log2(FC)| > 1.0
p-val < 0.05
E
BI+15% Cellu
BI+15% inWAX
Ferulic acid
M–Coumaric acid
Syringic acid
Phenolic acids
Hyocholic acid
Tauroursodeoxycholic acid
Taurocholic acid
Cholic acid
Bile acids
Z–score
F
GSH / GSSG
BI+15 %Cellu
BI+15% inWAX
G
(2R)-3-hydroxyisovaleroylcarnitine
(R)-butyrylcarnitine
Acetyl-l-carnitine
Adipoyl-l-carnitine
Decanoylcarnitine
Hexanoyl-l-carnitine
Octanoylcarnitine
Carnitine
LPC(18:2)
2-Thio PAF
LysoPC(14:0)
LysoPC(17:0)
LPC(16:0)
LysoPC(16:0)
LPCs

Figure 2

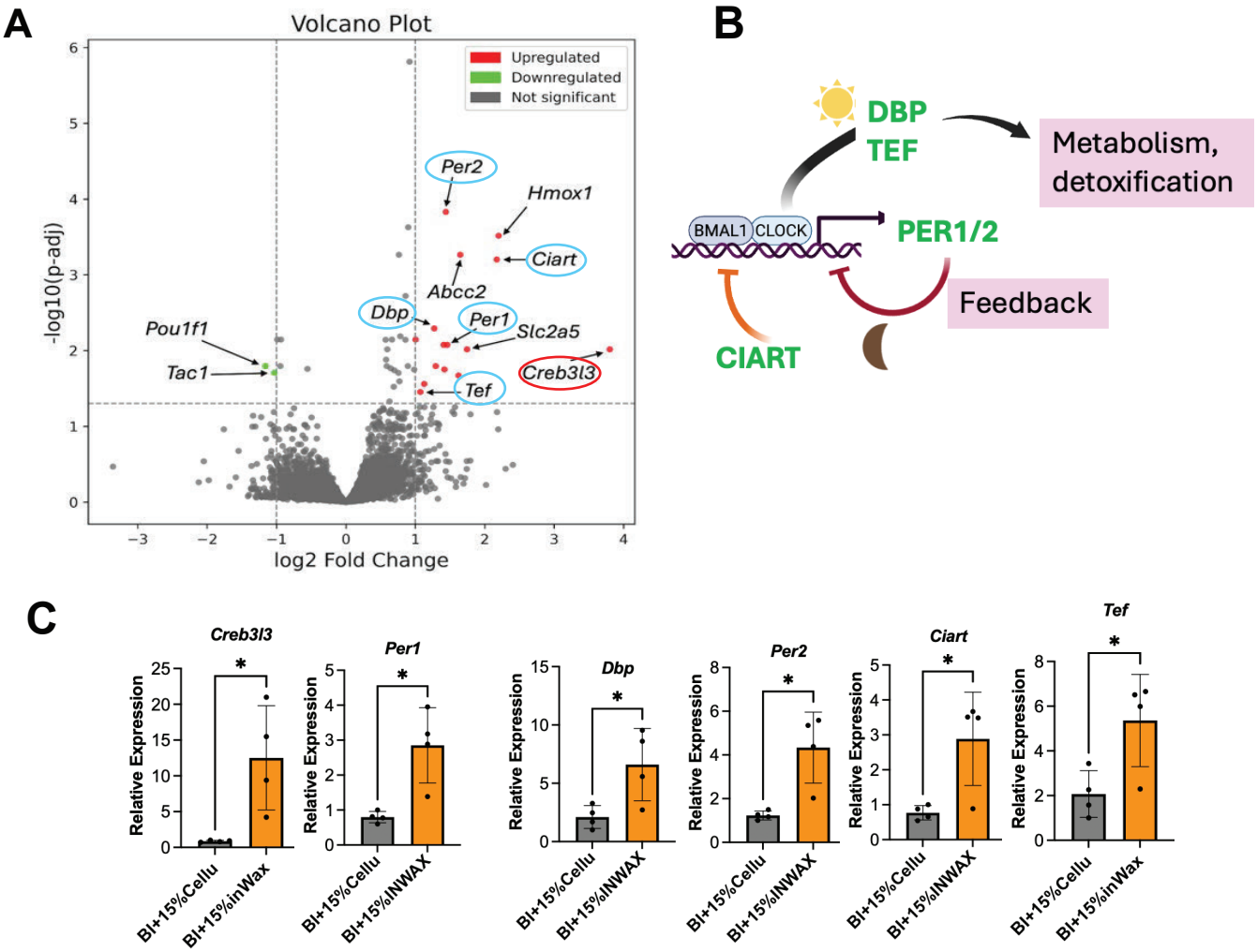
A
Volcano Plot
Upregulated
Downregulated
Not significant
Per2
Hmox1
Ciart
Abcc2
Dbp
Per1
Slc2a5
Pou1f1
Tac1
Creb3l3
Tef
-log10(p-adj)
log2 Fold Change
B
DBP
TEF
Metabolism, detoxification
BMAL1
CLOCK
PER1/2
Feedback
CIART
C
Creb3l3
Per1
Dbp
Per2
Ciart
Tef
Relative Expression
BI+15%Cellu
BI+15%inWax
BI+15%INWAX

Figure 3

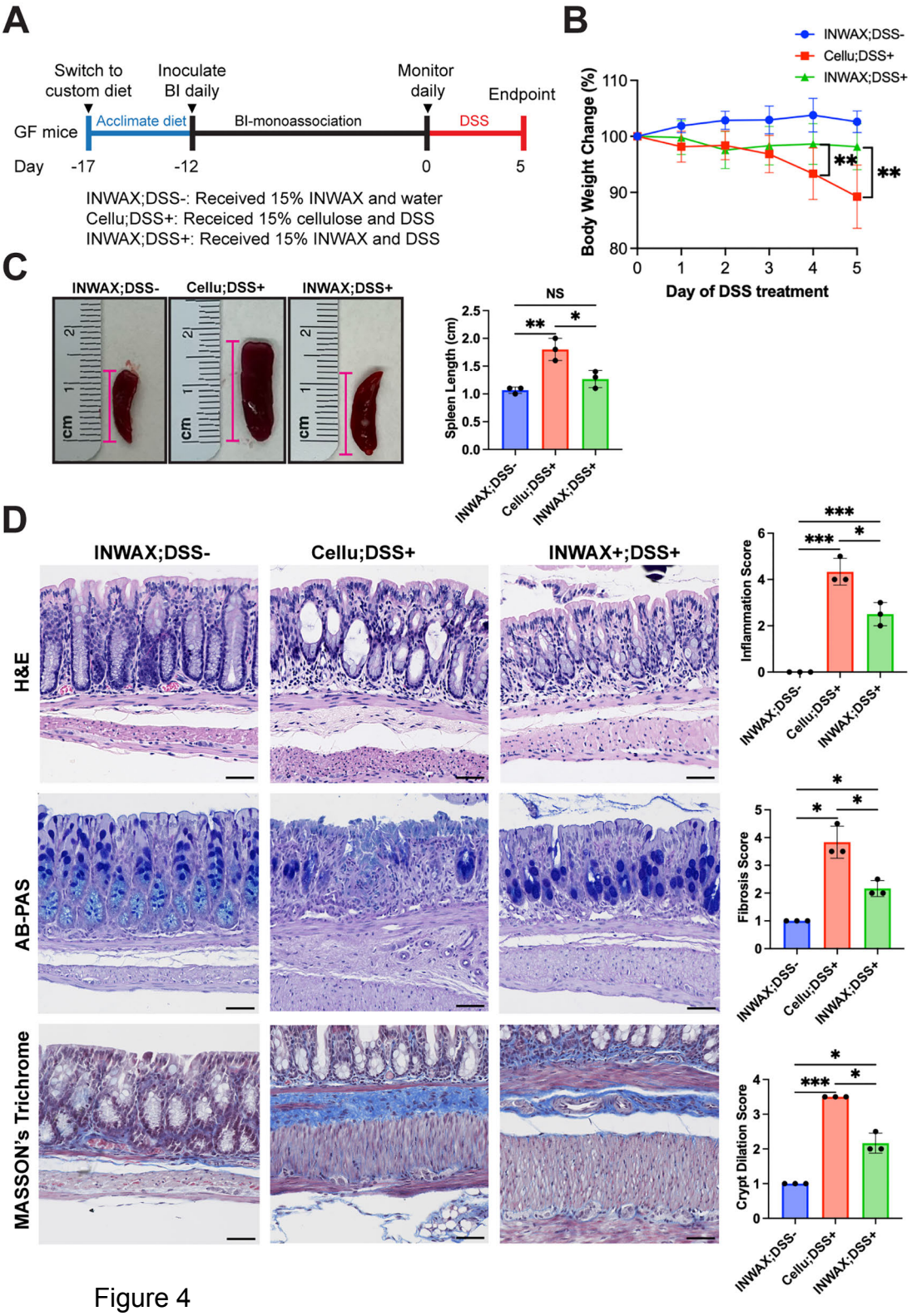
A
Switch to custom diet
Inoculate BI daily
Monitor daily
Endpoint
GF mice
Acclimate diet
BI-monoassociation
DSS
Day
-17
-12
0
5
INWAX;DSS-: Received 15% INWAX and water
Cellu;DSS+: Receiced 15% cellulose and DSS
INWAX;DSS+: Received 15% INWAX and DSS
B
INWAX;DSS-
Cellu;DSS+
INWAX;DSS+
Body Weight Change (%)
Day of DSS treatment
C
INWAX;DSS-
Cellu;DSS+
INWAX;DSS+
Spleen Length (cm)
NS
D
INWAX;DSS-
Cellu;DSS+
INWAX+;DSS+
H&E
AB-PAS
MASSON's Trichrome
Inflammation Score
Fibrosis Score
Crypt Dilation Score

Figure 4

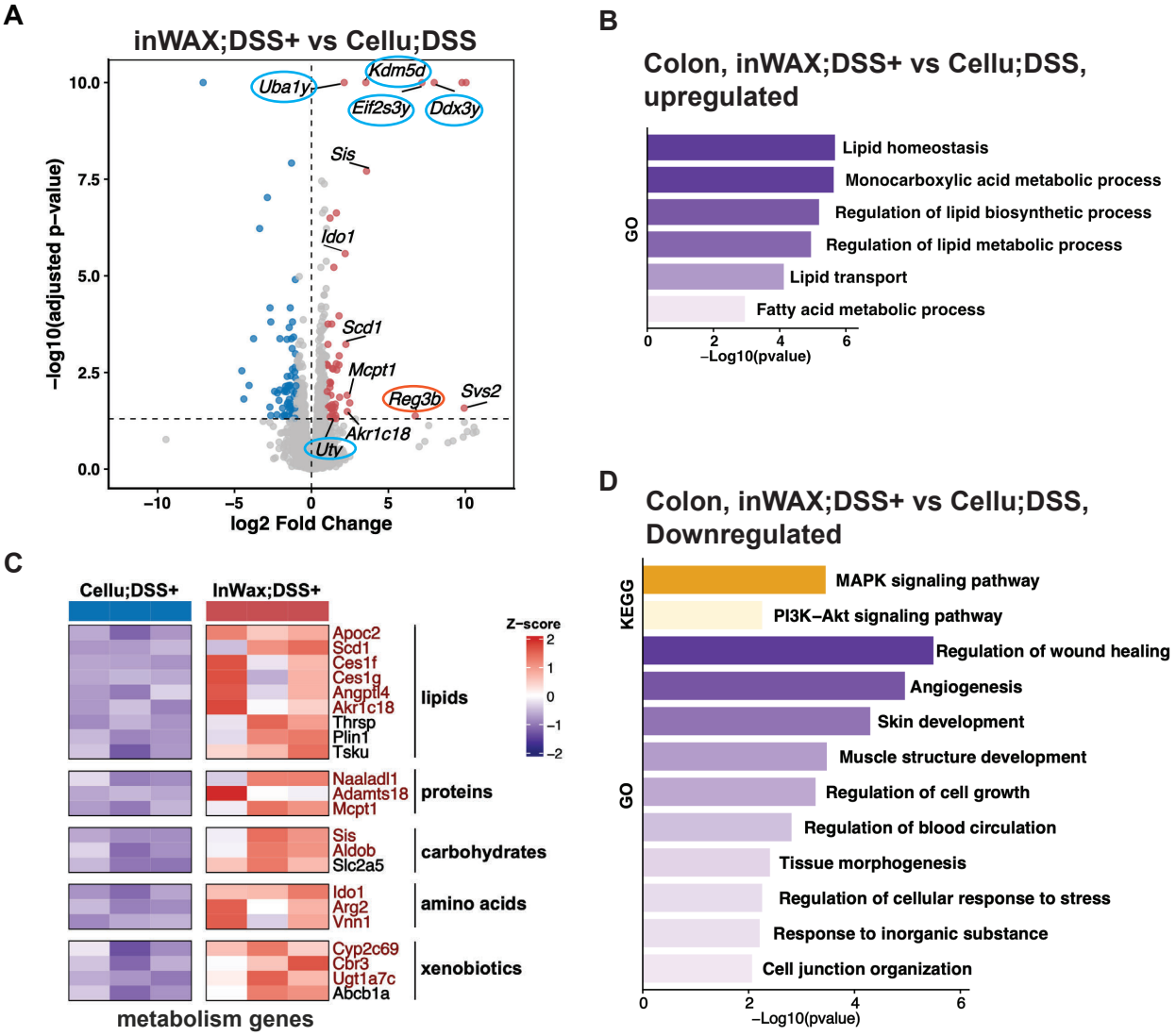
A
inWAX;DSS+ vs Cellu;DSS
Kdm5d
Uba1y
Eif2s3y
Ddx3y
Sis
Ido1
Scd1
Mcpt1
Reg3b
Svs2
Akr1c18
Uty
−log10(adjusted p−value)
log2 Fold Change
B
Colon, inWAX;DSS+ vs Cellu;DSS, upregulated
GO
Lipid homeostasis
Monocarboxylic acid metabolic process
Regulation of lipid biosynthetic process
Regulation of lipid metabolic process
Lipid transport
Fatty acid metabolic process
−Log10(pvalue)
C
Cellu;DSS+
InWax;DSS+
Z−score
Apoc2
Scd1
Ces1f
Ces1g
Angptl4
Akr1c18
Thrsp
Plin1
Tsku
lipids
Naaladl1
Adamts18
Mcpt1
proteins
Sis
Aldob
Slc2a5
carbohydrates
Ido1
Arg2
Vnn1
amino acids
Cyp2c69
Cbr3
Ugt1a7c
Abcb1a
xenobiotics
metabolism genes
D
Colon, inWAX;DSS+ vs Cellu;DSS, Downregulated
KEGG
MAPK signaling pathway
PI3K−Akt signaling pathway
GO
Regulation of wound healing
Angiogenesis
Skin development
Muscle structure development
Regulation of cell growth
Regulation of blood circulation
Tissue morphogenesis
Regulation of cellular response to stress
Response to inorganic substance
Cell junction organization
−Log10(pvalue)

Figure 5

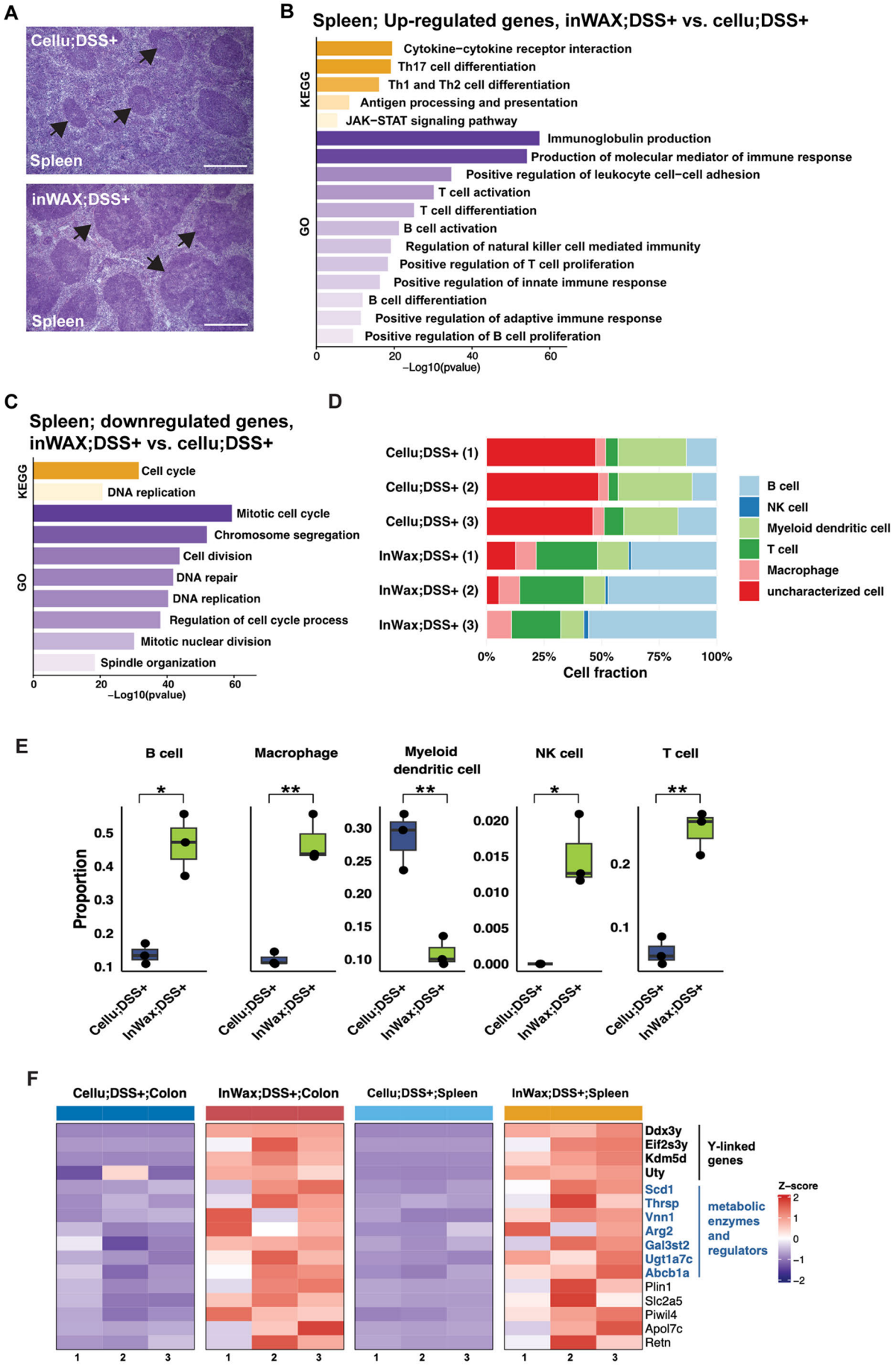
A
Cellu;DSS+
Spleen
inWAX;DSS+
Spleen
B
Spleen; Up-regulated genes, inWAX;DSS+ vs. cellu;DSS+
KEGG
Cytokine−cytokine receptor interaction
Th17 cell differentiation
Th1 and Th2 cell differentiation
Antigen processing and presentation
JAK−STAT signaling pathway
GO
Immunoglobulin production
Production of molecular mediator of immune response
Positive regulation of leukocyte cell−cell adhesion
T cell activation
T cell differentiation
B cell activation
Regulation of natural killer cell mediated immunity
Positive regulation of T cell proliferation
Positive regulation of innate immune response
B cell differentiation
Positive regulation of adaptive immune response
Positive regulation of B cell proliferation
0
20
40
60
−Log10(pvalue)
C
Spleen; downregulated genes, inWAX;DSS+ vs. cellu;DSS+
KEGG
Cell cycle
DNA replication
GO
Mitotic cell cycle
Chromosome segregation
Cell division
DNA repair
DNA replication
Regulation of cell cycle process
Mitotic nuclear division
Spindle organization
0
20
40
60
−Log10(pvalue)
D
Cellu;DSS+ (1)
Cellu;DSS+ (2)
Cellu;DSS+ (3)
InWax;DSS+ (1)
InWax;DSS+ (2)
InWax;DSS+ (3)
0%
25%
50%
75%
100%
Cell fraction
B cell
NK cell
Myeloid dendritic cell
T cell
Macrophage
uncharacterized cell
E
B cell
Macrophage
Myeloid dendritic cell
NK cell
T cell
Proportion
Cellu;DSS+
InWax;DSS+
F
Cellu;DSS+;Colon
InWax;DSS+;Colon
Cellu;DSS+;Spleen
InWax;DSS+;Spleen
Ddx3y
Eif2s3y
Kdm5d
Uty
Y-linked genes
Scd1
Thrsp
Vnn1
Arg2
Gal3st2
Ugt1a7c
Abcb1a
metabolic enzymes and regulators
Plin1
Slc2a5
Piwil4
Apol7c
Retn
Z-score
1
2
3

Figure 6

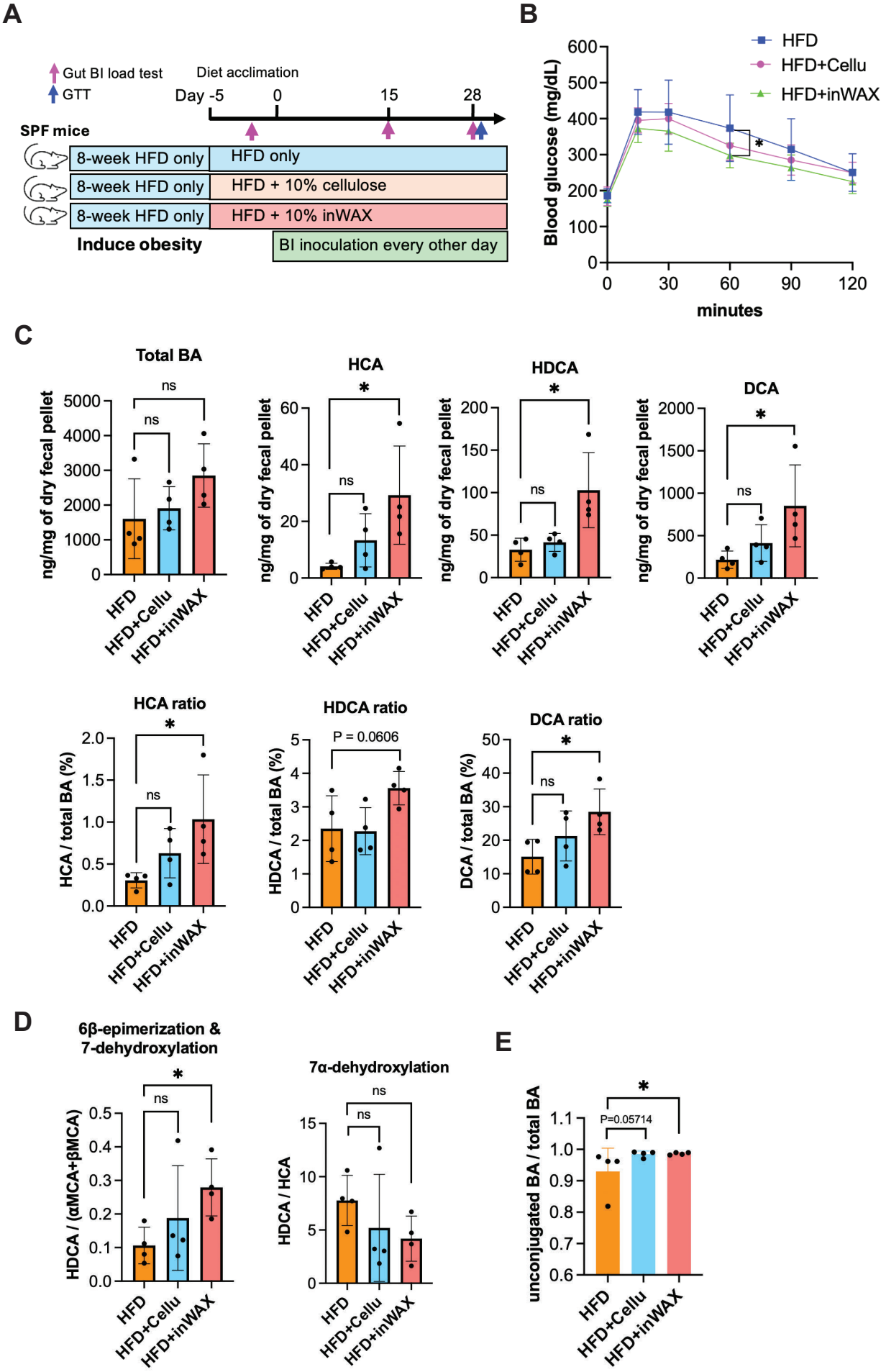
A
Gut BI load test
GTT
Diet acclimation
Day -5
0
15
28
SPF mice
8-week HFD only
HFD only
8-week HFD only
HFD + 10% cellulose
8-week HFD only
HFD + 10% inWAX
Induce obesity
BI inoculation every other day
B
HFD
HFD+Cellu
HFD+inWAX
Blood glucose (mg/dL)
minutes
C
Total BA
HCA
HDCA
DCA
ng/mg of dry fecal pellet
HCA ratio
HDCA ratio
DCA ratio
HCA / total BA (%)
HDCA / total BA (%)
DCA / total BA (%)
P = 0.0606
ns
D
6β-epimerization & 7-dehydroxylation
7α-dehydroxylation
HDCA / (αMCA+βMCA)
HDCA / HCA
E
unconjugated BA / total BA
P=0.05714

Figure 7

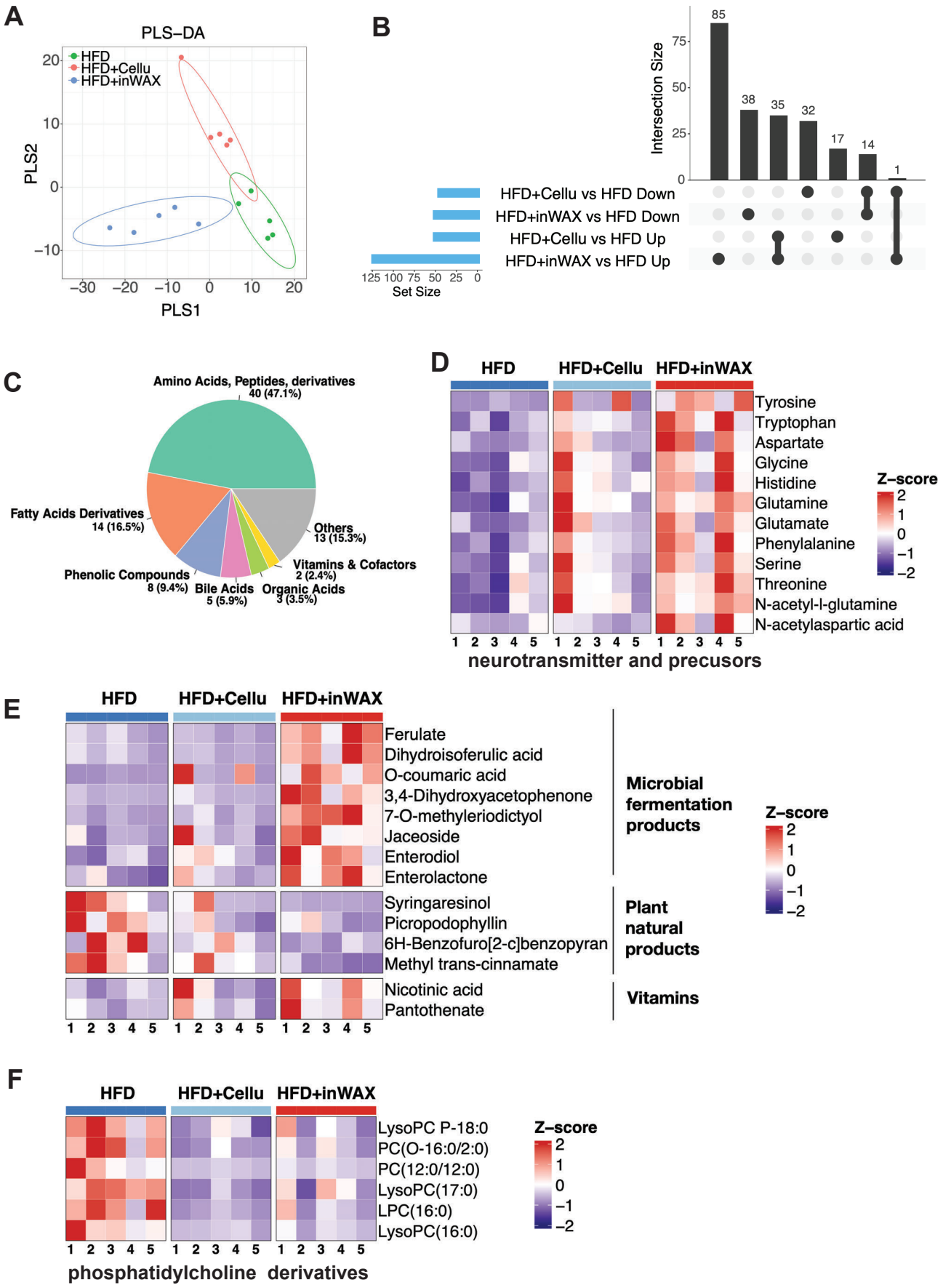
A
PLS–DA
HFD
HFD+Cellu
HFD+inWAX
PLS2
PLS1
B
Intersection Size
85
38
35
32
17
14
1
HFD+Cellu vs HFD Down
HFD+inWAX vs HFD Down
HFD+Cellu vs HFD Up
HFD+inWAX vs HFD Up
Set Size
C
Amino Acids, Peptides, derivatives 40 (47.1%)
Fatty Acids Derivatives 14 (16.5%)
Others 13 (15.3%)
Vitamins & Cofactors 2 (2.4%)
Phenolic Compounds 8 (9.4%)
Bile Acids 5 (5.9%)
Organic Acids 3 (3.5%)
D
HFD
HFD+Cellu
HFD+inWAX
Tyrosine
Tryptophan
Aspartate
Glycine
Histidine
Glutamine
Glutamate
Phenylalanine
Serine
Threonine
N-acetyl-l-glutamine
N-acetylaspartic acid
Z–score
neurotransmitter and precusors
E
HFD
HFD+Cellu
HFD+inWAX
Ferulate
Dihydroisoferulic acid
O-coumaric acid
3,4-Dihydroxyacetophenone
7-O-methyleriodictyol
Jaceoside
Enterodiol
Enterolactone
Microbial fermentation products
Syringaresinol
Picropodophyllin
6H-Benzofuro[2-c]benzopyran
Methyl trans-cinnamate
Plant natural products
Nicotinic acid
Pantothenate
Vitamins
Z–score
F
HFD
HFD+Cellu
HFD+inWAX
LysoPC P-18:0
PC(O-16:0/2:0)
PC(12:0/12:0)
LysoPC(17:0)
LPC(16:0)
LysoPC(16:0)
Z–score
phosphatidylcholine derivatives

Figure 8

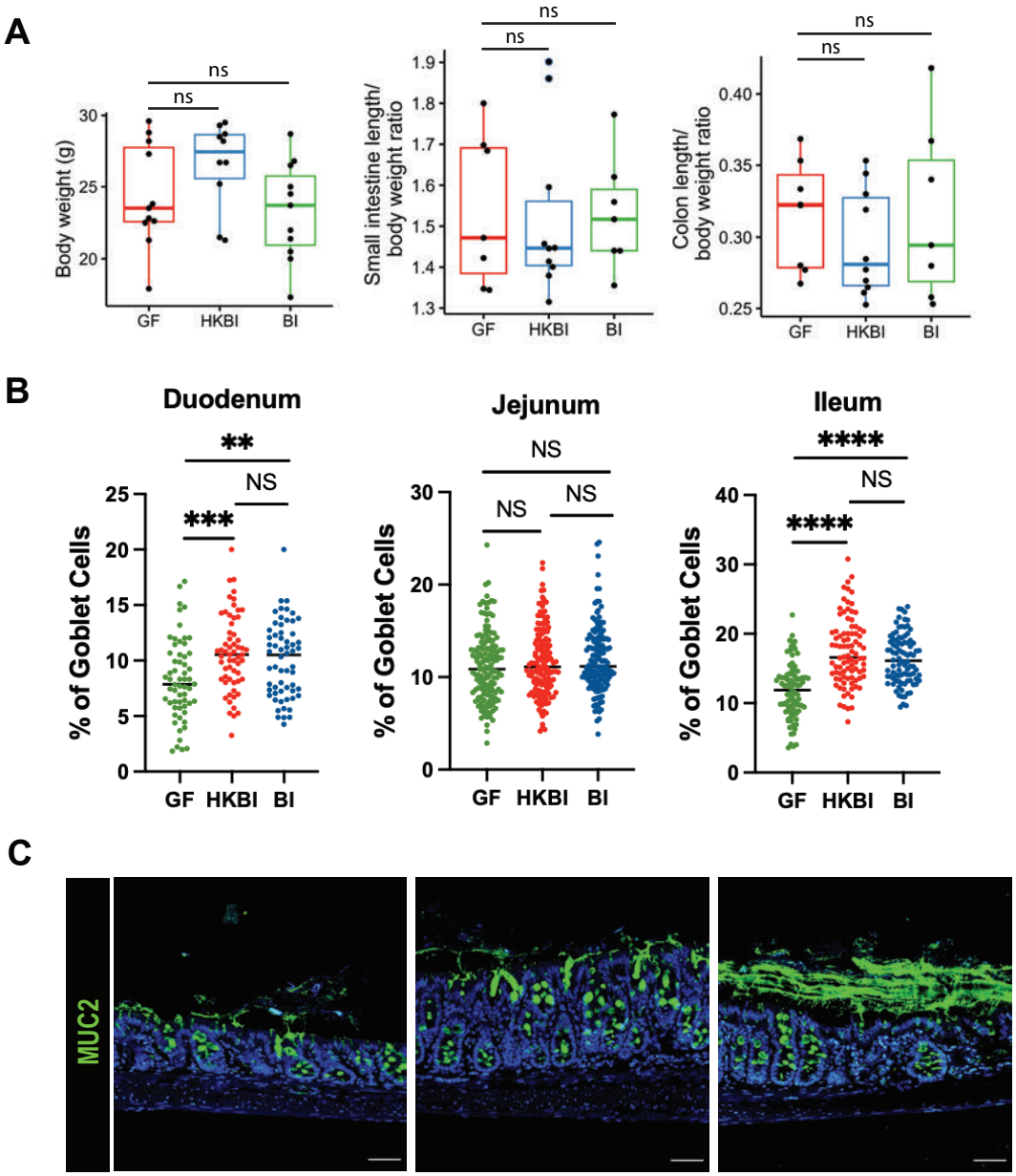

Figure S1. Physiological impact of BI monoassociation
(A) Quantification of body weight and the ratio of small intestine and colon length to body weight. (B) Quantification of goblet cells as a percentage of total colonic epithelial cells. (C) Representative immunofluorescence staining of MUC2 in the colon. Scale bars, 50 µm. ** $p < 0.01$; *** $p < 0.001$; **** $p < 0.0001$. ns, not significant.

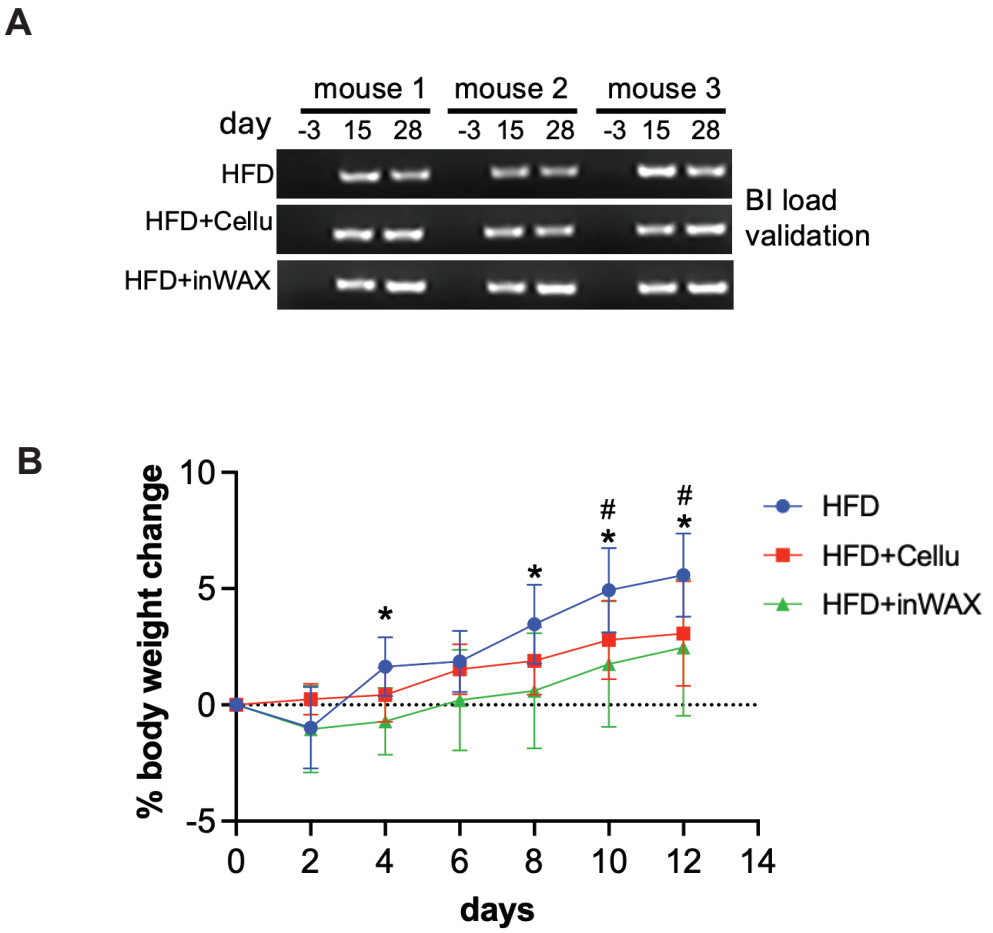

Figure S2. BI abudnace validation and difference in mouse body weight changes

(A) PCR validation of BI abundance in fecal samples of 3 mice in each group at the indicated time points. The first day of BI inoculation was designated as day 0. BI was undetectable prior to inoculation (day −3), indicating it is not a native resident of B6 mice.(B) Comparison of body weight change (%) during the first 12 days of BI inoculation. * indicates significance between HFD+inWAX and HFD. # indicates significance between HFD+cellu and HFD. * $p < 0.05$; # $p < 0.05$.

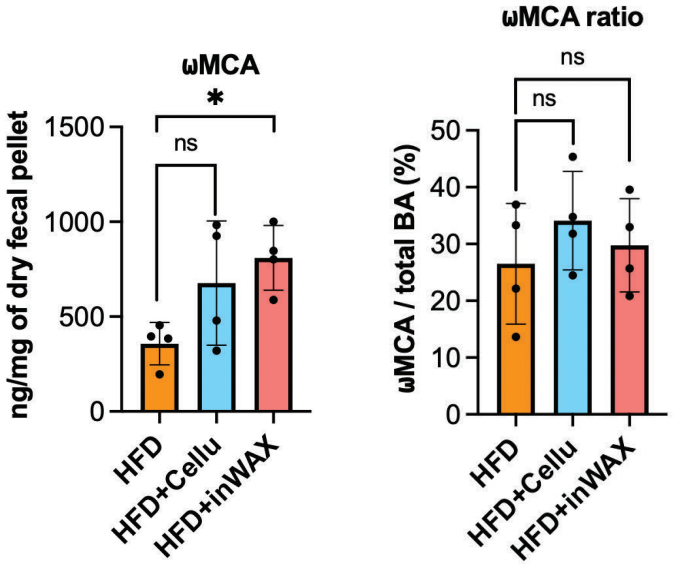

Figure S3. Fecal ωMCA concentrations and proportions to the total bile acid.
(A) Comparison of ωMCA concentrations. (B) Comparison of ωMCA proportions (%). * $p < 0.05$. ns, not significant

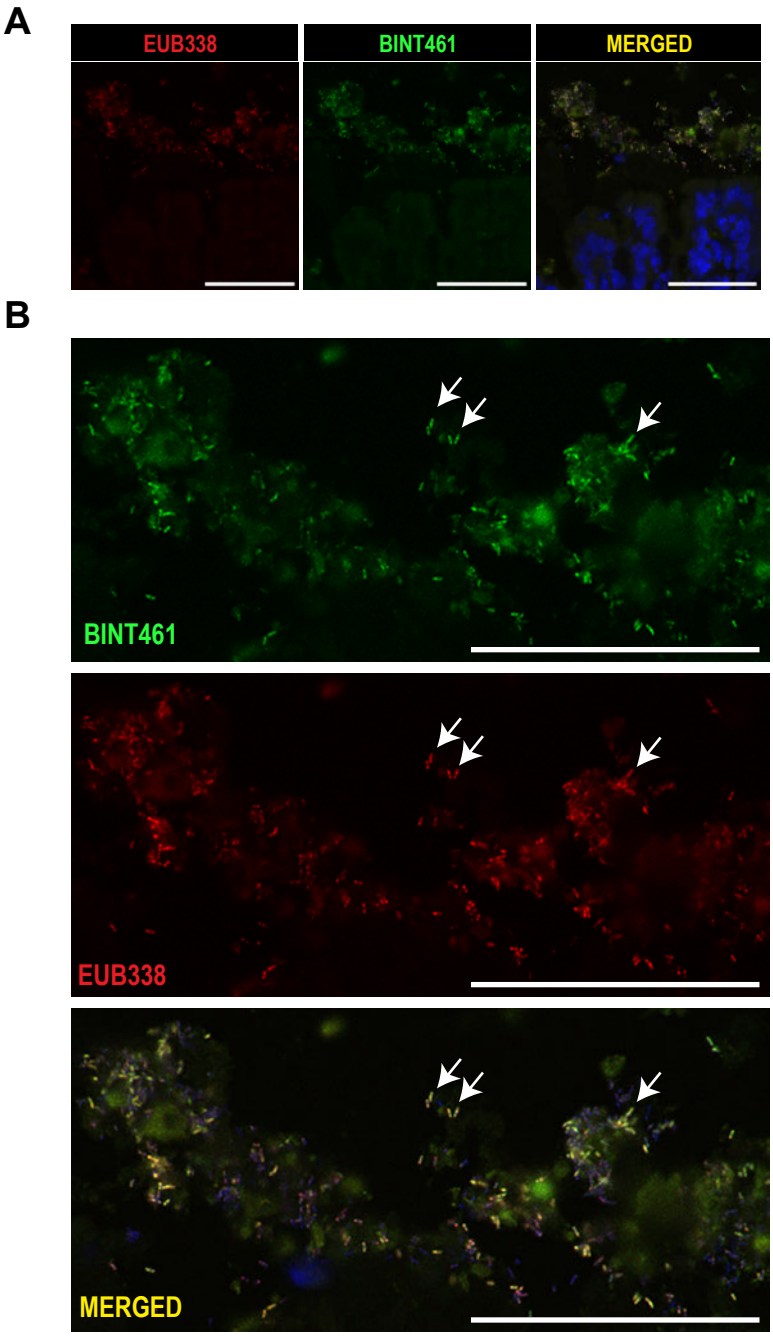

Figure S4. FISH detection of BI in the colonic lumen
(A) BI was detected using the BI-specific probe BNT461. The universal bacterial probe EUB338 served as a positive control. DAPI staining (blue) in the merged image labels colonic epithelial cell nuclei. (B) Higher-magnification views corresponding to the regions shown in (A). Arrows point to some BI. Scale bars, 50 μm.